Unravelling a mechanistic link between mitophagy defect, mitochondrial malfunction, and apoptotic neurodegeneration in MPS VII

Nishan Mandal[#1], Apurba Das[#1], and Rupak Datta[*1]

[1]Department of Biological Sciences, Indian Institute of Science Education and Research (IISER) Kolkata, Mohanpur, West Bengal, INDIA

[#] These authors contributed equally

[*] Author for correspondence:

Rupak Datta

E-mail: rupakdatta@iiserkol.ac.in

Tel: +91 033 6136 0000; Extn: 1214

ORCID identifier: 0000-0003-1820-9251

Summary

Progressive neurodegeneration and cognitive disability are prominent symptoms of MPS VII, a lysosomal storage disorder caused by β-glucuronidase enzyme deficiency. Yet, the mechanism of neurodegeneration in MPS VII remains elusive thereby limiting the scope of targeted intervention. To address this, we recently developed a β-glucuronidase-deficient (CG2135$^{-/-}$) *Drosophila* model of MPS VII. The CG2135$^{-/-}$ flies exhibited signs of neuromuscular degeneration, including loss of dopaminergic neurons, and accumulated engorged lysosomes, ubiquitinated proteins and mitochondria in their brains. These observations, coupled with our current finding that the CG2135$^{-/-}$ flies were highly susceptible to starvation, prompted us to investigate potential defects in the autophagy-lysosomal clearance machinery in the fly brain. We found that both autophagy induction and lysosome-mediated autophagosomal turnover were impaired in the CG2135$^{-/-}$ fly brain. This was evidenced by lower Atg8a-II levels, reduced Atg1 and Ref(2)P expression along with accumulation of lipofuscin-like inclusions and multilamellar bodies. Interestingly, mitophagy was also found to be defective in their brain, causing buildup of enlarged mitochondria with distorted cristae and reduced membrane potential. This, in turn, affected mitochondrial function as reflected by drastically reduced brain ATP levels. Energy depletion triggered apoptosis in neuronal as well as non-neuronal cells of the CG2135$^{-/-}$ fly brain, where we also detected TUNEL-positive dopaminergic neurons. Resveratrol treatment, previously found to protect against loss of dopaminergic neurons in the CG2135$^{-/-}$ flies, has now been shown act by correcting the mitophagy defect and preventing ATP depletion. Collectively, our study establishes a causal link between mitophagy defect, mitochondrial malfunction, and neurodegeneration in MPS VII.

Key words:

MPS VII, autophagy, mitophagy, neurodegeneration, energy depletion, apoptosis, resveratrol

Introduction

Mucopolysaccharidosis VII (MPS VII) is a recessively inherited lysosomal storage disorder caused by mutations in the *β-glucuronidase* (*β-GUS*) gene. β-GUS is one of the eleven glycosaminoglycan (GAG)-catabolizing lysosomal hydrolase, deficiency of which results in accumulation of undegraded or partially degraded GAGs in the lysosomes [1,2]. MPS VII patients suffer from progressive multiorgan dysfunction, and most of them eventually succumb to premature death. Common clinical manifestations of MPS VII include, hydrops fetalis, short stature with coarse face and skeletal deformities, heart valve abnormality, hepato-splenomegaly, and recurrent infections [1–3]. Additionally, MPS VII patients also develop a variety of neurological symptoms like mental retardation, limited vocabulary, delayed speech, hearing impairment and restricted movement [3,4]. This indicates that MPS VII patients suffer from neurodegeneration, which was corroborated by autopsy studies showing extensive lysosomal storage in different regions of the patient's brain [5]. The MPS VII mouse model also exhibited accumulation of storage vacuoles throughout the brain and signs of neurodegeneration in the hippocampus and cerebral cortex regions that worsened with age [6]. However, the molecular and cellular events that connect lysosomal storage to neurodegeneration in MPS VII are still not well-understood. Without this knowledge, developing a mechanism-based therapy to alleviate neurological problems of MPS VII patients remains an unmet need. This issue has become even more critical because enzyme replacement therapy (ERT), the only approved treatment for MPS VII patients, despite being successful in alleviating some of the symptoms, has not yet been shown to resolve the neurological complications [7,8]. This is most likely due to the limited ability of the infused enzyme to cross the blood brain barrier [8]. All these challenges emphasize the urgent need for an in-depth study of the brain pathology and the mechanism of neurodegeneration in MPS VII that would facilitate exploration of small molecule-based therapy.

Towards this goal, recently we developed the first *Drosophila* model of MPS VII by knocking-out the fly *β-GUS* gene (*CG2135*) [9]. The CG2135$^{-/-}$ fly exhibited progressive locomotor disability, attributed to neuromuscular degeneration. Compared to the wild type counterparts, the CG2135$^{-/-}$ fly brain displayed distinctive features like, extensive vacuolation, abnormal buildup of engorged lysosome as well as ubiquitinated proteins and an increased abundance of mitotracker-positive vesicles. Interestingly, a significant loss of dopaminergic neurons was also observed in the CG2135$^{-/-}$ fly brain [9]. Dopaminergic

84 neurons are classically known to control locomotion and their depletion is associated with movement
85 disorders such as Parkinson's disease [10,11]. These initial findings provided us with an excellent platform
86 for delving deeper into the underlying mechanism of neurodegeneration in MPS VII.

87 In line with our observation in the CG2135$^{-/-}$ fly brain, Martins *et. al.* previously reported mitochondrial
88 accumulation in the MPS IIIC mouse brain. Their data also revealed a progressive decline in activities
89 of some of the respiratory chain enzymes in mitochondria isolated from the MPS IIIC mice brain [12].
90 Apart from these two MPS disorders, mitochondrial accumulation in brain was also reported in animal
91 models of few other unrelated lysosomal storage disorders, e.g. Gaucher disease, multiple sulfatase
92 deficiency and CLN7 [13–15]. In this context, it is worth mentioning that, due to their high energy demand,
93 neuronal cells rely heavily on mitochondrial quality control to maintain a healthy and efficient pool of
94 mitochondria. These quality control mechanisms include biogenesis of mitochondria, their
95 fusion/fission dynamics and selective clearance of damaged mitochondria through the mitophagy
96 pathway [16]. Aberrations in these processes have been reported to play a causative role in many
97 neurodegenerative diseases [17,18]. However, very little is known about the mechanistic link between
98 mitochondrial quality control in the brain and neurodegeneration associated with MPS disorders in
99 general, and MPS VII in particular.

100 In this study, we systematically investigated the cause and consequence of abnormal buildup of
101 mitochondria in the CG2135$^{-/-}$ fly brain to better understand the mechanism of neurodegeneration in
102 MPS VII. We initially focused on the autophagy-lysosomal clearance pathway in the brain to check if
103 any defect in this machinery led to inefficient turnover of mitochondria. This notion was fuelled by our
104 previously reported observation of aberrant autophagy in the CG2135$^{-/-}$ larvae [19]. A similar defect was
105 also reported in β-GUS deficient chondrocyte cell line [20]. Autophagy is a coordinated cellular waste
106 disposal system in which cell debris is packed into double-membrane autophagosome vesicles and
107 targeted to lysosome for degradation and recycling [21]. The process involves a series of autophagy-related
108 genes (Atg) and proteins which are regulated by various physiological cues [22]. Apart from bulk
109 autophagy, there are specialized forms of autophagy such as ER-phagy or mitophagy, via which
110 damaged cellular organelles are specifically degraded [18,23]. We first suspected that the adult CG2135$^{-/-}$

111 flies might be suffering from a gross autophagy defect when we found them to be significantly more
112 susceptible to starvation than their wild type counterparts. Following this lead, we confirmed that
113 autophagy is indeed compromised in the CG2135$^{-/-}$ fly brain. Further probing uncovered that the process
114 of mitophagy was also impaired in the CG2135$^{-/-}$ fly brain, resulting in the accumulation of abnormally
115 large mitochondria with deformed cristae structure and decreased membrane potential. This led to
116 significant drop in ATP levels, inducing extensive apoptotic cell death in the CG2135$^{-/-}$ fly brain, with
117 signs of apoptosis also evident in the dopaminergic neurons. Treatment with resveratrol, previously
118 shown to prevent loss of dopaminergic neurons in the CG2135$^{-/-}$ flies, has now been found to protect
119 the CG2135$^{-/-}$ fly brain from mitophagy defect and ATP exhaustion. Our findings thus establish a
120 mechanistic link between mitophagy defect, mitochondrial malfunction, and neurodegeneration in MPS
121 VII.

122 **Results**

123 **Defective autophagy-lysosome clearance system in CG2135$^{-/-}$ fly brain**

124 During initial characterization of the MPSVII fly (CG2135$^{-/-}$), we observed an abnormal accumulation
125 of mitotracker-positive puncta and ubiquitinated proteins in their brain, indicating a potential defect in
126 the lysosome-mediated cellular clearance system [9]. In a follow-up study, we reported aberrant
127 autophagy in the CG2135$^{-/-}$ larvae [19]. These findings prompted us to analyze the status of autophagy in
128 the adult CG2135$^{-/-}$ fly, specifically in its brain, to better understand the mechanism of
129 neurodegeneration in this fly model. Autophagy pathway is known to be activated as a protective
130 response to nutrient starvation [24]. Studies with various model organisms have established that an
131 autophagy defect results in enhanced susceptibility to starvation [25–27]. Taking cue from these reports, we
132 compared the starvation sensitivity of the adult CG2135$^{-/-}$ flies with their age-matched wild-type
133 counterparts. For this, we took wild type (W^{1118}) and CG2135$^{-/-}$ flies of different age groups (young flies
134 - 4 days old, middle-aged flies - 15 days old and old flies - ≥ 30 days old) and subjected them to a no-
135 food condition. The percentage survivability was analyzed every 12 hours by counting the number of
136 surviving flies (Figure 1A). The survival curves, as well as the mean survival time (MST) under starved
137 condition, clearly showed that the CG2135$^{-/-}$ flies were more susceptible to starvation than the wild type

138 flies at all ages (Figures 1B-1D). This data strongly indicated that the adult CG2135$^{-/-}$ flies could be
139 suffering from an autophagy defect. We then shifted our focus to a detailed analysis of the autophagy
140 status in the CG2135$^{-/-}$ fly brain. For this, we collected the wild type and CG2135$^{-/-}$ flies of different age
141 groups (4-days old to 45-days old) and examined the level of Atg8a, the *Drosophila* homolog of
142 mammalian LC3, in their brains. Atg8a is considered as a reliable marker for autophagy as it gets
143 recruited to autophagosome vesicles in its phosphatidylethanol amine (PE) conjugated form [28].Our
144 western blot data clearly showed a marked reduction in the Atg8a-II levels (the PE-conjugated form of
145 Atg8a that correlates with the autophagosome abundance) in the CG2135$^{-/-}$ fly brain as compared to
146 their wild type counterparts across all age groups. Notably, the differences in brain Atg8a-II levels
147 between the wild type and the CG2135$^{-/-}$ fly progressively increased with age (Figures 2A and 2B).
148 Consistent with this finding, immunofluorescence staining of whole fly brains with an Atg8a antibody
149 showed a significant reduction in the Atg8a-positive autophagic vesicles in 30-days old CG2135$^{-/-}$ fly
150 brain compared to age-matched wild type flies (Figures. S1A-F). In this context, it is worth noting that
151 although there was no significant difference in the Atg8a transcript levels between the wild type and the
152 CG2135$^{-/-}$ fly brains, the Atg8a-I protein level (the non-autophagosome bound form of Atg8a) was also
153 found to be reduced in the CG2135$^{-/-}$ fly brains (Figures S1G – S1I). To ascertain the reason behind the
154 reduced abundance of autophagosomes in the CG2135$^{-/-}$ fly brain, we checked the status of the Ref(2)P,
155 the fly homologue of the mammalian autophagic cargo adapter protein p62/SQSTM1 [29]. As evident
156 from our whole-brain immunofluorescence staining and western blot data, the Ref(2)P protein level in
157 the CG2135$^{-/-}$ fly brain was significantly less as compared to the wild type flies of similar age (Figures
158 2C – 2I). To study if lowering of the Ref(2)P protein level is due to transcriptional downregulation, we
159 analyzed the Ref(2)P mRNA level by RT-qPCR and found it to be significantly reduced in the CG2135^{-}
160 $^{/-}$ fly brain (Figure 2J). This prompted us to also check the expression of Atg1, one of the important
161 autophagy initiation genes [30]. Interestingly, almost 60% decline in the transcript level of Atg1 was
162 observed in the CG2135$^{-/-}$ fly brain as compared to their age-matched wild type counterparts (Figure
163 2K). Collectively, these data indicate that a defect in the autophagy induction might be the underlying
164 reason behind the reduced abundance of the autophagosomes in the old CG2135$^{-/-}$ fly brain. We also
165 noticed that in stark contrast to the wild type flies, the optical lobe and midbrain region of the 45-days

166 old CG2135$^{-/-}$ flies exhibited distinctive autofluorescence when imaged in the FITC channel (Figures
167 2L – 2N). Such autofluorescent puncta are reminiscent of lipofuscin, the storage granules of undegraded
168 lipids and misfolded proteins that accumulate in the lysosomes of postmitotic neurons [31]. Accumulation
169 of lipofuscin is a hallmark of ageing and also has been reported in many neurodegenerative diseases [32–
170 34]. This intriguing finding prompted us to further analyze the tissue architecture of the fly brains using
171 high resolution transmission electron microscopy (TEM). Our TEM images revealed that compared to
172 the wild type flies, the CG2135$^{-/-}$ fly brains contained very few double-membrane autophagosome
173 vesicles but instead had an abundance of multilamellar bodies (MLBs) with whorl-like structures
174 (Figures 2O–2S). Abnormal accumulation of MLBs has been observed in a variety of lysosomal storage
175 disorders, resulting from dysfunction of lysosomal hydrolytic activity [33,35,36]. Considering all these
176 findings, it is evident that there are multiple defects in the autophagy-lysosome clearance pathway in
177 the CG2135$^{-/-}$ fly brain.

178 **Abnormal accumulation of enlarged and damaged mitochondria in the CG2135$^{-/-}$ fly brain**

179 One of the unexplained pathological features of the CG2135$^{-/-}$ fly brain is the increased accumulation
180 of MitoTracker-stained puncta [9]. Upon further analysis, we noted that in the 30-days old CG2135$^{-/-}$ fly
181 brain there was a significant increase in the MitoTracker staining intensity (by ~ 1.9 folds) as well as
182 the size of the MitoTracker-positive puncta (by ~ 1.3 folds) compared to the wild type fly brain (Figures
183 3A-3F). The level of the mitochondrial protein ATP5A was also significantly elevated in the CG2135$^{-/-}$
184 fly brain, as revealed from our western blot analysis (Figure S2). Taken together, these data indicated
185 an increased abundance of mitochondrial mass in the CG2135$^{-/-}$ fly brain. To gain deeper insights, we
186 next performed ultrastructure analysis of the mitochondria in the 45-days old fly brains using TEM
187 (Figures 3G and 3H). Examination of the TEM images revealed that compared to the wild type fly brain,
188 there was ~ 1.6 folds increase in the average mitochondria size in the CG2135$^{-/-}$ fly brain (0.27 μm^2 vs.
189 0.43 μm^2) (Figure 3I). Percent frequency distribution analysis of the mitochondria size further revealed
190 that the smaller mitochondria (< 0.2 μm^2) were much more abundant in the wild type fly brain compared
191 to their CG2135$^{-/-}$ counterparts (~ 46% in the wild type vs. ~ 17% in the CG2135$^{-/-}$ fly brain). In contrast,
192 the CG2135$^{-/-}$ fly brain had an increased number of enlarged mitochondria of sizes ≥ 0.4 μm^2 (~ 21%

193 in the wild type vs. ~ 44% in the CG2135$^{-/-}$ fly brain). Abundance of intermediate sized mitochondria
194 (0.2 μm^2 - 0.4 μm^2) was also slightly higher in the CG2135$^{-/-}$ fly brain than the wild type (Figure 3J).
195 Aged mitochondria often exhibit distorted cristae structure and are found to be functionally
196 compromised [37]. This prompted us to methodically examine the mitochondrial ultrastructure from the
197 TEM images and categorized them into healthy, intermediate-damaged, and damaged mitochondria
198 based on the integrity of their cristae structure (Figures 3K-3M). Our analysis revealed that in the wild
199 type fly brain, over 70% of the mitochondria were healthy with orderly packed cristae, whereas, the
200 percentage of healthy mitochondria in the CG2135$^{-/-}$ fly brain was only ~ 45%. In contrast, the CG2135^{-}
201 $^{/-}$ fly brain exhibited a higher abundance of the damaged and intermediate-damaged mitochondria
202 compared to their wild type partners (damaged: 30% in the CG2135$^{-/-}$ vs. 14% in the wild type,
203 intermediate damaged: 25% in the CG2135$^{-/-}$ vs. 14% in the wild type) (Figure 3N). Having confirmed
204 the abundance of enlarged and damaged mitochondria in the CG2135$^{-/-}$ fly brain, our next goal was to
205 understand its cause and functional consequences.

206 **Impaired mitophagy in the CG2135$^{-/-}$ fly brain**

207 Mitochondria are particularly susceptible to oxidative damage due to continuous ROS production
208 during cellular respiration. As a cellular cleansing mechanism, the damaged mitochondria are
209 eliminated through the process of mitophagy, a specialized form of autophagy [16,17]. In this context, it is
210 important to note that impairment of mitophagy has been reported in several age-related
211 neurodegenerative diseases [18]. These prior reports, combined with our finding that autophagy is
212 suppressed in the CG2135$^{-/-}$ fly brain, led us to investigate whether these flies also suffer from a
213 mitophagy defect. For this, 45 days old fly brains were co-stained with LysoTracker (green) and
214 MitoTracker (red), and the mitophagy status was analysed by quantifying the extent of colocalization
215 of lysosomes and mitochondria from confocal images. Data presented in Figures 4A-4H clearly shows
216 that, compared to the wild type flies, there was a significantly reduction in the lysosome-mitochondria
217 colocalization in the CG2135$^{-/-}$ fly brain, indicating a mitophagy defect in these flies. This was further
218 corroborated by our TEM images, which showed fewer autophagosome-bound mitochondria that the
219 45-day-old CG2135$^{-/-}$ fly brain compared to their wild type counterparts (Figures 4J and 4L). As an

220 alternative approach to analyse mitophagy, we isolated the mitochondria-rich fraction from 45 days old
221 fly brains and checked for the presence of Atg8a -II, an autophagosome-bound protein, in that fraction.
222 Our western blot data showed that the Atg8a -II protein levels in the mitochondria-rich fraction isolated
223 from the CG2135$^{-/-}$ fly brain was significantly lower than in the age-matched wild type flies (Figures
224 4M-4O). Taken together, our data suggest that impaired mitophagy is the reason behind the
225 accumulation of enlarged and damaged mitochondria in the CG2135$^{-/-}$ fly brain. This prompted us to
226 investigate the mitochondrial function in the CG2135$^{-/-}$ fly brain, particularly in terms of energy
227 production.

228 **CG2135$^{-/-}$ fly suffers from brain energy deficit**

229 Mitophagy plays a neuroprotective role by maintaining mitochondrial homeostasis, thereby ensuring
230 sufficient ATP supply for proper brain function [38,39]. Since mitochondrial membrane potential (ΔΨm) is
231 a key indicator of functionally active mitochondria and is essential in driving ATP synthesis, we opted
232 to measure ΔΨm in the mitophagy-deficient 45 days old CG2135$^{-/-}$ fly brain using JC-1 assay [40].
233 Compared to the age-matched wild type flies, we observed a ~ 40% reduction in the red-to-green
234 fluorescence ratio in the CG2135$^{-/-}$ fly brain, indicating a significant decrease in ΔΨm in these flies
235 (Figures 5A-5G). Strikingly, the ATP levels in the 45 days old CG2135$^{-/-}$ fly brain was found to be
236 reduced by >50% than in the wild type fly brain (Figure 5H). This data indicates that the older CG2135^{-}
237 $^{/-}$ flies suffer from severe brain energy deficit, which may be the trigger for neurodegeneration in these
238 flies. ATP is produced in the mitochondrial inner membrane by the enzyme ATP synthase, which utilizes
239 the proton gradient across the mitochondrial membrane as the driving force for generating ATP [40]. It has
240 been reported that if ΔΨm is compromised for some reason, ATP synthase reverses its direction acting
241 as an ATP-consuming enzyme to translocate protons from the mitochondrial matrix to the
242 intermembrane space. In such situations, the expression of ATPase Inhibitory Factor 1 (ATPIF1) is
243 upregulated to prevent wasteful ATP expenditure by inhibiting the ATP synthase activity [41]. Consistent
244 with these findings, we observed a significant upregulation of ATPIF1 transcript level in the 45 days
245 old CG2135$^{-/-}$ fly brain, suggesting that ATP synthase activity is indeed inhibited in these flies, possibly
246 to counteract further depletion of ATP levels (Figure 5I).

Increased apoptosis in the CG2135$^{-/-}$ fly brain

We previously reported prominent signs of neurodegeneration, including loss of dopaminergic neurons, in the CG22135$^{-/-}$ fly brains [9]. However, the mechanism underlying this neurodegeneration is far from clear. Since mitochondrial damage and ATP depletion have been reported to induce apoptotic cell death in both neuronal and non-neuronal cells, we checked the status of apoptosis in the energy-deficient 45 days old CG2135$^{-/-}$ fly brain [42–44]. Our western blot data clearly showed that the CG2135$^{-/-}$ fly brains had significantly elevated levels of cleaved-caspase-3, a key mediator of apoptosis (Figures 6A an 6B) [45]. Interestingly, co-immunostaining of the fly brains with antibodies against cleaved-caspase-3 and ELAV (a pan-neuronal marker) [46] revealed that both neuronal (ELAV-positive) as well as non-neuronal (ELAV-negative) cells in the CG2135$^{-/-}$ fly brain showed signs of apoptosis (Figure S3). These findings were corroborated by transcript analysis of the proapoptotic factor Hid[47], which showed ~ 2.4 folds upregulation in the CG2135$^{-/-}$ fly brain compared to their aged-matched counterparts (Figure 6C). For direct visualization of DNA fragmentation in apoptotic cells, we next performed TUNEL staining in whole mount brains. We observed ~ 2.8 folds increase in the abundance of TUNEL-positive cells in the 45 days old CG2135$^{-/-}$ fly brains compared to the wild type fly brains (Figures 6D-6L). When the brains were co-stained with anti-Tyrosine Hydroxylase antibody (to mark the dopaminergic neurons) and TUNEL (to mark the apoptotic nuclei), we observed that ~ 18% of the dopaminergic neurons in the CG2135$^{-/-}$ fly brains were TUNEL positive, as compared to only ~ 2% in the wild type flies (Figures 6M-6S). Collectively, these data suggests that apoptosis plays a key role in neurodegeneration in the MPS VII fly.

Resveratrol treatment corrects mitophagy defect and prevents ATP loss in the CG2135$^{-/-}$ fly brain

We previously reported that resveratrol treatment reversed the locomotor deficit in the CG2135$^{-/-}$ fly and protected against loss of their dopaminergic neurons [9]. But how these abnormalities were corrected by resveratrol remained a mystery. To evaluate the mechanism of resveratrol action, we treated the CG2135$^{-/-}$ flies with it for 30-45 days starting from day 4 post-eclosion. We then assessed the status of Atg1 transcript and the level of mitochondrial protein ATP5A in the brain. We found that Atg1 transcript level, which was significantly downregulated in the CG2135$^{-/-}$ fly brain, was completely restored to the

274 normalcy in the resveratrol-treated CG2135$^{-/-}$ flies (Figure 7A). The elevated ATP5A level in the
275 CG2135$^{-/-}$ fly brain was also reduced to the to the basal level upon resveratrol treatment (Figures 7B
276 and 7C). Most importantly, resveratrol treatment protected the CG2135$^{-/-}$ flies from brain energy deficit
277 by completely restoring their ATP levels (Figure 7D). From our data, it can be conjectured that
278 correction of mitophagy defect and restoration of ATP levels in the CG2135$^{-/-}$ fly brain upon resveratrol
279 treatment is the mechanistic basis for its neuroprotective effect.

280 **Discussion**

281 Despite being known as a debilitating disease with prominent neurological symptoms, the mechanism
282 of neurodegeneration in MPS VII remains poorly understood. The work presented here aimed to bridge
283 this knowledge gap by employing a *Drosophila* model of the disease (the CG2135$^{-/-}$ fly). We report a
284 gross defect in the autophagy-lysosome clearance pathway in the CG2135$^{-/-}$ fly brain, which also
285 manifested as impaired mitophagy. As a consequence, there was an accumulation of structurally
286 deformed and functionally compromised mitochondria leading to bioenergy deficit in the brain and
287 apoptotic neurodegeneration. We also demonstrated that mitophagy defect and brain energy deficit in
288 the CG2135$^{-/-}$ fly could be corrected by treatment with resveratrol, providing a potential explanation for
289 its neuroprotective property.

290 Autophagy is crucial for maintaining cellular homeostasis by clearing cytotoxic protein aggregates and
291 damaged organelles, a process especially vital for post-mitotic cells like neurons in the central nervous
292 system (CNS) [21,48]. In fact, defective autophagy has been linked with neurodegenerative diseases like
293 Alzheimer's, Parkinson's, and ALS [48]. Lysosomal storage disorders (LSDs) such as multiple sulfatase
294 deficiency, Gaucher disease and mucolipidosis type IV, often exhibit neurodegeneration in brain with
295 impaired autophagy [13,14,33]. Despite these studies, the status of autophagy in the MPS VII brain remained
296 completely unexplored. Even for other MPS disorders, there is hardly any systematic study on brain
297 autophagy. We, therefore, took up this challenge following the lead from our earlier observation of
298 defective autophagy in the CG2135$^{-/-}$ larvae [19]. Also, in the present study, the adult CG2135$^{-/-}$ flies were
299 found to be highly susceptible to starvation. Since autophagy is typically induced as a survival response
300 under nutrient starvation, this starvation-sensitivity was an indicator of a global autophagy defect in the

301 CG2135$^{-/-}$ flies [25,26]. However, as autophagic response is highly tissue-specific and it is known that
302 starvation-induced autophagy in brain is much less pronounced than in other tissues [49], it was imperative
303 for us to specifically analyze the autophagy status in the adult CG2135$^{-/-}$ fly brains. A significantly
304 reduced abundance of Atg8a-II protein, a bona fide marker of autophagosomes, confirmed that
305 autophagy is indeed altered in the CG2135$^{-/-}$ fly brains. It was interesting to note that the Atg8a-II levels
306 in the wild type fly brains gradually increased with age, indicating normal autophagy induction but
307 progressive decline of lysosome-mediated autophagosome turnover leading to autophagosome
308 accumulation [50,51]. But, the Atg8a-II levels in the CG2135$^{-/-}$ fly brains did not increase with age and
309 remained almost at the basal level throughout. This result, together with our data demonstrating
310 significantly reduced expression of Atg1 and Ref(2)P in the CG2135$^{-/-}$ fly brains, suggest impaired
311 autophagy induction in the MPS VII flies. The process of autophagy is fine-tuned by multilayered
312 regulation of Atg1/ULK1 initiation factor [52]. Various transcription factors (like ATF4, FoxO3, STAT1,
313 and ZKSCAN3) and signal transducers (like mTOR and AMPK) have been shown to regulate the
314 expression and activity of Atg1/ULK1[53,54]. It remains to be seen whether altered expression of any of
315 these regulatory proteins is responsible for downregulation of Atg1 in the CG2135$^{-/-}$ fly brains.
316 Atg1/ULK1, once activated, initiates autophagy by phosphorylating its downstream targets leading to
317 the assembly of Atg12-Atg5-Atg16L1 complex. It acts as a E3 ligase, facilitating lipidation of cytosolic
318 Atg8a-I/LC3-1 to autophagosome-bound Atg8a-II/LC3-II [50]. So, it is not surprising that under the
319 condition of suppressed Atg1 expression, Atg8a-II levels remained consistently low at all ages in the
320 CG2135$^{-/-}$ fly brains. The low transcript as well as protein levels of Ref(2)P in the CG2135$^{-/-}$ fly brains
321 was rather intriguing. Ref(2)P, the fly orthologue of the mammalian autophagic cargo adaptor protein
322 p62, usually accumulates when there is a block in the autophagy pathway [55]. However, a contrasting
323 observation was reported in peripheral blood mononuclear cells (PBMCs) from Gaucher disease
324 patients, where LC3-II levels as well as p62 transcript were both found to be reduced compared to
325 PBMCs from healthy donor [56]. This suggest that Ref(2)P/p62 expression and autophagy induction could
326 be simultaneously impaired under certain conditions, although physiological implication of such
327 phenomenon is not clear. Ref(2)P/p62 being a TFEB-inducible gene, its reduced expression in the
328 CG2135$^{-/-}$ fly brains might be a collateral consequence of TFEB downregulation [57]. While TFEB has

329 been found to be dysregulated in some neurodegenerative diseases [58], its status is not known in any of
330 the MPS disorders and this remains a future area for investigation.

331 In addition to stunted autophagy induction, defective clearance of the autophagosomal content was also
332 evident in the CG2135$^{-/-}$ fly brains, as indicated by accumulation of lipofuscin-like inclusions and
333 multilamellar bodies (MLBs). Lipofuscin is an intralysosomal autofluorescent material mainly
334 composed of lipids and misfolded proteins that are resistant to lysosomal degradation. Lipofuscin
335 accumulation can be aggravated when lysosomal degradation process is hampered, particularly in
336 certain lysosomal storage diseases such as Batten disease, Tay-Sachs disease and Sanfilippo syndrome
337 [32,59,60]. Accumulation of concentric multilamellar structures in the CG2135$^{-/-}$ fly brains is another
338 signature for dysfunctional lysosomal activity, as has been observed in the brains of a *Drosophila* model
339 of mucolipidosis type IV and fibroblasts form Parkinson's disease patients [33,35,61].

340 Autophagy being a critical homeostatic machinery in neuronal as well as some non-neuronal cells of
341 the central nervous system [62–64], blockage in multiple steps of this pathway in the CG2135$^{-/-}$ fly brains
342 was expected to have deleterious consequences. This notion was validated when we found significantly
343 reduced mitochondria-lysosome colocalization and fewer autophagosome-sequestered mitochondria in
344 the CG2135$^{-/-}$ fly brains, indicating a defect in mitophagy, a specialized form of autophagy to remove
345 damaged mitochondria. As the primary site for cellular energy production, mitochondria are prone to
346 oxidative damage [17]. This vulnerability is even more pronounced in high energy-demanding tissues like
347 the brain [65]. To maintain a healthy pool of mitochondria, cells are endowed with a robust mitochondrial
348 quality control mechanism that comprises two opposing but coordinated processes: mitochondrial
349 biogenesis, and removal of damaged mitochondria through mitophagy [16,17]. The canonical mitophagy is
350 mediated by the PINK1-Parkin signalling cascade. In this pathway, PINK1 is stabilized on the
351 mitochondrial outer membrane, following which it phosphorylates and recruits Parkin, thereby
352 triggering ubiquitin-dependent mitophagy [16]. In PINK1-Parkin-independent non-canonical mitophagy,
353 adaptor molecules on the mitochondrial membrane, such as FUNDC1, can directly initiate mitophagy
354 [66,67]. It has been reported that Atg1/ULK1 plays a vital role in regulating mitophagy through both
355 canonical and non-canonical pathways by phosphorylating key molecules like Parkin or FUNDC1 [67–

356 [70]. Thus, it can be speculated that reduced Atg1 expression in the CG2135$^{-/-}$ fly brains is responsible, at
357 least in part, for the observed mitophagy defect. Decreased p62/Ref(2)P levels may also contribute to
358 impaired mitophagy, as p62/Ref(2)P downregulation has been shown to cause autophagic cargo loading
359 failure [71]. Furthermore, PINK1-Parkin-mediated mitophagy is reported to depend on p62/Ref(2)P [72],
360 suggesting that reduced levels of this cargo adapter protein could aggravate the mitophagy defect in the
361 CG2135$^{-/-}$ fly brains.

362 The mitophagy defect in the CG2135$^{-/-}$ fly brains provided an explanation for the accumulation of
363 enlarged mitochondria with deformed cristae structure and reduced ΔΨm. It is well-documented that
364 such excessive buildup of damaged mitochondria is a direct consequence of a mitophagy defect,
365 regardless of the actual cause of the defect [73,74]. It is noteworthy that while signs of autophagy defect
366 were evident even in the younger CG2135$^{-/-}$ flies, accumulation of damaged and depolarized
367 mitochondria in their brains could be detected only in the older flies, aged 30 days and beyond. In fact,
368 the brains of 45days-old CG2135$^{-/-}$ flies were found to bioenergetically inefficient showing nearly a
369 50% drop in ATP levels. Such mitophagy deficiency-induced depletion of ATP levels in the brain has
370 been observed in other neurodegenerative diseases [75,76], but not reported earlier in any of the MPS
371 disorders. Since ΔΨm is a key driver for ATP synthesis [40], it can be inferred that ATP depletion in the
372 CG2135$^{-/-}$ fly brains is primarily due to accumulation of depolarized mitochondria with significantly
373 reduced ATP-synthesizing ability. Consumption of ATP via reversal of ATP synthase activity, as often
374 occurs in depolarized mitochondria [41], may further exhaust the ATP levels in the CG2135$^{-/-}$ fly brains.
375 Robust upregulation of ATPIF1 transcript level in the CG2135$^{-/-}$ fly brains support this possibility.
376 Under conditions of compromised ΔΨm, ATPIF is known to act as an inhibitor of ATP synthase activity,
377 preventing ATP wastage [41].

378 Depleted levels of intracellular ATP is an established determinant of apoptotic cell death [44,77]. Thus, it
379 was not unexpected that ATP depletion in a high energy demanding tissue like brain would induce
380 apoptotic cell death in the CG2135$^{-/-}$ flies. Multiple reports have confirmed that autophagy machinery
381 plays a crucial pro-survival role and defects in this process predispose cells to apoptosis [78–80]. Therefore,
382 in addition to ATP depletion, autophagy impairment could be another factor for inducing apoptosis in

the CG2135$^{-/-}$ fly brains. Earlier, we reported a significant loss of dopaminergic neurons in the CG2135$^{-/-}$ fly brains, which could be mitigated with resveratrol treatment [9]. However, the underlying cause of this neuronal loss and the mechanism by which resveratrol conferred protection against it remained unclear. The cause of neuronal loss became evident when we discovered that neuronal cells, particularly the dopaminergic neurons, are undergoing apoptosis in the CG2135$^{-/-}$ fly brains. This finding mirrors one of the hallmarks of Parkinson's disease, which is characterized by progressive loss dopaminergic neurons via apoptosis [81]. It is worth noting that dopaminergic neurons have a high metabolic demand due to their extensive axonal network and dopamine secretory activity, making them particularly vulnerable to energy crisis [82]. Intriguingly, we observed that resveratrol treatment could correct the mitophagy defect and fully restore ATP levels in the CG2135$^{-/-}$ fly brains, providing a mechanistic explanation for its neuroprotective property. These findings align with an earlier report demonstrating that resveratrol provides neuroprotection by safeguarding against rotenone-induced mitochondrial damage through the enhancement of autophagic activity [83].

Apart from neuronal cells, signs of apoptosis were also found in some non-neuronal cells of the CG2135$^{-/-}$ fly brains. In *Drosophila* brain, non-neuronal cells are predominantly glial cells, which play crucial roles in maintaining and protecting neural environment [84]. Whether degeneration of glial cells also drives neurodegeneration in MPS VII remains an open question. It has been observed that degenerating glial cells derived from MPS II mouse were able to promote neuronal death in a co-culture condition [85]. Given that the role of mitophagy in glial cells has been implicated in the pathogenesis of other neurodegenerative diseases [86,87], it may be worthwhile to investigate the contributions of these cells in neurodegeneration associated with MPS VII and related disorders.

To conclude, the work presented here significantly advances our understanding of the pathogenesis of MPS VII by uncovering a previously unknown mechanistic link between mitophagy defect, mitochondrial malfunction leading to brain energy deficits, and apoptotic neurodegeneration. We also identified some molecular alterations in the autophagy-lysosomal pathway in the MPS VII fly brains, which may provide novel therapeutic leads for pharmacological interventions. The promising results

with resveratrol in correcting the mitophagy defect and preventing loss of ATP levels could be a significant initial step towards this direction.

Acknowledgements

This research was supported by the Ministry of Education, Government of India grant STARS/APR2019/BS/779/FS awarded to RD. The authors express their sincere gratitude to Prof. Mohit Prasad and the members of his fly lab for providing the facilities and technical inputs in fly maintenance. The authors also thank Dr. Sankar Maiti, Dr. Arnab Gupta and Prof. Jayasri Das Sarma for sharing critical reagents. Additionally, Dr. Arnab Gupta is thanked for providing access to his confocal microscopy facility. The authors acknowledge helpful suggestions received from Dr. Sudipta Bar and Dr. Subhankar Dolai for his critical comments on the manuscript. Mr. Abhrajyoti Nandi, Mr. Sujoy Bose and Mr. Subhajit Majumdar are appreciated for their help with fly maintenance and other technical assistance. The authors acknowledge the support of the TEM facility at the Institute of Life Sciences (ILS), Bhubaneswar. NM was supported by CSIR fellowship and AD was supported by DBT and ICMR-SRF fellowships.

Author contributions

N.M. A.D. and R.D. conceptualized the work and designed the experiments; N.M. and A.D. performed the experiments; N.M. A.D. and R.D. analysed the data; N.M. A.D. and R.D. wrote the manuscript; R.D. supervised the work and acquired the funding.

Declaration of interests

The authors declare no competing interests

Supplemental information

Figure S1 – S3

Figure legends

Figure 1: **CG2135$^{-/-}$ flies are significantly more susceptible to starvation**

(A) Schematic representation of experimental setup for starvation assay.

(B-D) Wild type (WT) and CG2135$^{-/-}$ flies of different ages (4, 15 and 30 days old) were subjected to starvation for varying duration and survival curves were plotted. The filled circles represent WT and the empty squares represent CG2135$^{-/-}$. Mean survivability time (MST) was calculated and the respective values are mentioned at the bottom of each curve. The survival curves as well as the MST values indicate that the CG2135$^{-/-}$ flies were significantly more susceptible to starvation than their wild type counterparts. All experiments were done independently (N=3), and the total flies analysed n≥130.

Error bars represent the standard error of mean (SEM). MST means mean survivability time (hours). Asterisks represent level of significance (****$P \leq 0.0001$, **$P \leq 0.01$, *$P \leq 0.05$; Student's *t*-test).

Figure 2: Defective autophagy-lysosome clearance system in the CG2135$^{-/-}$ fly brain

(A) Immunoblot of Atg8a showing the protein level of Atg8a-II (14 kDa) from head lysate of WT and CG2135$^{-/-}$ of different ages (4,15,30 and 45 days old). α-Tubulin (54 kDa) was considered as the loading control.

(B) The bar graph represents the quantification for Atg8a-II/Tubulin band intensity showing reduced level of Atg8a II in CG2135$^{-/-}$compared to age-matched WT head lysate. (N=3)

(C-F) Immunostaining of Ref(2)P in the 30-day-old mid-brain of WT and CG2135$^{-/-}$ with anti-Ref(2)P (green) showed reduced Ref(2)P aggregates in CG2135$^{-/-}$. Nucleus was counterstained with DAPI (blue).

(G)The bar graph depicts the mean fluorescence intensity of Ref(2)P of WT and CG2135$^{-/-}$. (N≥4 fly brain of each genotype).

(H) Immunoblot of Ref(2)P (100 kDa) from 30 days old WT and CG2135$^{-/-}$ head lysate showed a reduced level of the protein in CG2135$^{-/-}$. α-Tubulin (54 kDa) was considered as the loading control.

(I) The bar graph showing the relative level of the Ref(2)P/Tubulin protein. The protein is downregulated in the CG2135$^{-/-}$. (N=3)

(J) The Ref(2)P transcript level in 30 days WT and CG2135$^{-/-}$ was determined by RT-qPCR and normalised to RP49 as housekeeping gene control. (N=3)

(K) The Atg1 transcript level in 30 days WT and CG2135$^{-/-}$ was determined by RT-qPCR and normalised to RP49 as housekeeping gene control. (N=3)

(L-N) Autofluorescence bodies in 45 days WT and CG2135$^{-/-}$ showed an increase in CG2135-/- and their quantification represented a bar graph. The bodies have been detected using the FITC channel and images were acquired in Apotome.2. (N=4 fly brains of each genotype)

(O-P) Electron micrograph showing autophagosome and multilamellar bodies from 45 days WT and CG2135$^{-/-}$ brain. (Q-R) Shows the higher magnified images from the respective insets.

(S) Quantification of the number of multilamellar bodies compared between WT and CG2135$^{-/-}$ has been represented as a bar graph. Multiple fields were analysed from 3 brains of each genotype. The CG2135$^{-/-}$ had increased multilamellar bodies than WT.

All experiments were done independently. Error bars represent the standard error of mean (SEM). Asterisks represent a level of significance (****$P \leq 0.0001$, **$P \leq 0.01$, *$P \leq 0.05$; Student's *t*-test).

Figure 3: Accumulation of enlarged and damaged mitochondria in the CG2135$^{-/-}$ fly brain

(A-D) Optic lobes of 30 days WT and CG2135$^{-/-}$ fly brain stained with mitotracker red (showing mitochondria in red) and Hoechst (marking the nucleus in blue), indicating mitochondrial accumulation CG2135$^{-/-}$ fly brain compared to age-matched WT fly.

(E-F) Quantification of mitotracker intensity and the size of the mitotracker positive puncta showing increased mitochondrial mass with puncta size in CG2135$^{-/-}$ fly brain compared to WT flies. (N ≥ 5 fly brain)

(G-H) Electron micrographs of 45 days WT and CG2135$^{-/-}$ fly brains showing mitochondria marked with white arrow. The mitochondrial number has increased in CG2135$^{-/-}$ fly brain.

(I-J) Quantification of the individual mitochondrial area and percent frequency distribution of different sizes shows the accumulation of larger mitochondria in the CG2135$^{-/-}$ (N=276 mitochondria from 3 independent experiments) fly brain compared to age-matched WT fly brain (N=245 mitochondria from

3 independent experiments). Multiple fields were analysed for measuring the size of the mitochondria using ImageJ.

(K-M) Mitochondria observed under TEM are categorized as healthy, intermediate, and completely damaged based on their cristae structure, as shown in Figures K, L, and M respectively.

(N) The percentage of healthy, intermediate-damaged, and completely damaged mitochondria was quantified from multiple fields of three independent experiments showing reduced healthy but increased damaged mitochondria in the CG2135$^{-/-}$ fly brain.

All experiments were done independently. Error bars represent the standard error of mean (SEM). Asterisks represent a level of significance (****$P \leq 0.0001$, **$P \leq 0.01$, *$P \leq 0.05$; Student's *t*-test).

Figure 4: Impaired mitophagy in the CG2135$^{-/-}$ fly brain

(A-H) Mitotracker-lysotracker co-staining at 45 days old fly brain showing fewer colocalisation spots (yellow puncta) in 45 days CG2135$^{-/-}$ fly brain indicating reduced mitophagy. Only mitotracker positive puncta is indicated with white arrows, and puncta positive for both lysotracker and mitotracker (yellow puncta) is marked with yellow arrows. Hoechst is used for counterstaining of the nucleus.

(I) Pearsons' colocalisation coefficient (PCC) analysis shows reduced lysotracker-mitotracker colocalization in the optic lobe of the CG2135$^{-/-}$ fly brain compared to WT type (N ≥ 7 fly brain).

(J-L) Electron micrograph of 45-day-old WT and CG2135$^{-/-}$ fly brains showing reduced mitochondria-containing autophagy vesicle (K) in the CG2135$^{-/-}$ fly brain as indicated by white arrow.

(M) Verification of mitochondria-rich fraction isolated from the 45-day fly head by western blot of mitochondrial protein, ATP5A (55 kDa), and cytosolic marker GAPDH (36 kDa).

(N) The immunoblot against anti-Atg8a showed reduced Atg8a-II protein in isolated mitochondria-rich fraction from CG2135$^{-/-}$ fly head compared to WT. ATP5A was considered as the loading control.

(O) The bar graph shows the quantification for the Atg8a-II/ATP5A. N=3

All experiments were done independently. Error bars represent the standard error of mean (SEM). Asterisks represent a level of significance (****$P \leq 0.0001$, *$P \leq 0.05$; Student's *t*-test).

Figure 5: Reduced mitochondrial membrane potential and ATP level in CG2135$^{-/-}$ fly brain.

(A-F) The optic lobes of 45 days WT and CG2135$^{-/-}$ fly brains were stained with JC1 dye.

(G) Quantification of the red/green ratio showed reduced membrane potential in CG2135$^{-/-}$ brain compared to age-matched WT fly. (N ≥ 16 fly brain from each genotype)

(H) Quantification of total ATP from 45-day-old fly head. (N = 3), showing significantly reduced ATP levels in the CG2135$^{-/-}$ fly brains.

(I) Relative expression of ATPIF1 in 45 days old CG2135$^{-/-}$ fly brain (N=4).

All experiments were done independently. Error bars represent the standard error of mean (SEM). Asterisks represent a level of significance (**$P \leq 0.01$, *$P \leq 0.05$; Student's *t*-test).

Figure 6: Increased apoptosis in the CG2135$^{-/-}$ fly brain.

(A) Immunoblot of Cleaved-caspase 3 using anti-Cleaved-caspase 3 showed increased protein at 45 days old CG2135$^{-/-}$ fly head. α-Tubulin (54 kDa) was considered as the loading control.

(B) The bar graph represents the Cleaved-caspase 3/Tubulin. N=3

(C) Relative transcript level of pro-apoptotic gene Hid determined by RT-qPCR, increased in CG2135$^{-/-}$ fly head compared to age-matched 45 days old WT fly. (N=3)

(D) TUNEL staining of 45 days old WT and CG2135$^{-/-}$ brain, DAPI used for marking the nucleus.

(J) Quantification of the TUNEL-positive nucleus revealed increased TUNEL-positive cells in CG2135$^{-/-}$ fly brain. (N=4 fly brain)

(K-P) Co-staining with TUNEL and anti-TH (tyrosine hydroxylase) showed elevated TUNEL-positive dopaminergic neurons in 45 days CG2135$^{-/-}$ compared to age-matched WT brain.

(Q) The bar graph representing quantification of apoptotic dopaminergic neurons in WT and CG2135$^{-/-}$. (N=5 fly brain of each genotype)

All experiments were done independently. Error bars represent the standard error of mean (SEM). Asterisks represent level of significance (**$P \leq 0.01$, *$P \leq 0.05$; Student's *t*-test).

532 **Figure 7: Resveratrol treatment rescues MPS VII pathologies by restoring ATP level**

533 (A) The bar graph represents the Atg1 transcript level determined by RT-qPCR in 30-day-old
534 resveratrol-treated WT, and CG2135$^{-/-}$ fly head showing restoration of Atg1 level. The gene expression
535 was normalised to RP49 as housekeeping gene control. (N=3)

536 (B-C) The immunoblot and its quantification represented by the bar graph using anti-ATP5A showed
537 rectification of mitochondrial accumulation in brain by resveratrol treatment of CG2135$^{-/-}$ fly compared
538 with untreated. (N=4).

539 (D) The bar graph represents the ATP level on resveratrol treatment at 45 days. ATP level in CG2135$^{-/-}$
540 fly head restored to normalcy on resveratrol treatment compared to untreated. (N ≥ 3)

541 All experiments were done independently. Error bars represent the standard error of mean (SEM).
542 Asterisks represent a level of significance (****$P \leq 0.0001$, ***$P \leq 0.001$, *$P \leq 0.05$; Student's *t*-test).

543 **Materials and methods**

544 All the reagents are enlisted in the resource table.

545 **Key resource table:**

Reagent or Resource	Source	Identifier
Antibodies		
anti-GABARAP [1:1000 (WB), 1:100 (IF)]	Cell signalling technology	Cat no.: E1J4E
anti-Ref(2)P [1:1000 (WB), 1:500 (IF)]	Abcam	Cat no.: ab178440
Anti-ATP5A [1:10000]	Abcam	Cat no.: ab14748
Anti-Cleaved Caspase-3 [1:750 (WB), 1:75 (IF)]	Cell signalling technology	Cat no.: 9661
Anti-α-Tubulin [1:5000 (WB)]	Biobharati	Cat no.: BB-AB0118
Anti-Elav [1:100]	DSHB	Cat no.: Elav-9F8A9
Anti-tyrosine-hydroxylase [1:500]	Millipore	Cat no.: AB152
Goat Anti-Rabbit Alexa-488	Thermo scientific	Cat no.: A11008
Goat Anti-rabbit Alexa-568	Thermo scientific	Cat no.: A11011
Goat Anti-mouse Alexa-488	Thermo scientific	Cat no.: A11001
Goat Anti-mouse Alexa-568	Thermo scientific	Cat no.: A11031
Goat Anti-Rabbit I_gG-Peroxidase	Sigma Aldrich	Cat no.: A9169

Goat Anti-Mouse I_gG-Peroxidase	Sigma Aldrich	Cat no.: A9044
Chemicals		
Vectashield	Vecta laboratories	Cat no.: H1000
Mitotracker	Invitrogen	Cat no.: M7513
Lysotracker DND green	Invitrogen	Cat no.: L7526
JC1	Invitrogen	Cat no.: T3168
TUNEL	Merck	Cat no.: 12156792910
ATP Determination kit	Invitrogen	Cat no.: A22066
Trizol	Ambion	Cat no.: 15596026
cDNA kit	Thermo scientific	Cat no.: AB1453A
DNase	Thermo scientific	Cat no.: 18068-015
SYBR green	Biorad	Cat no.: 1725121
Protease inhibitor cocktail	Sigma Aldrich	Cat no.: S8830
Triton-X100	Sigma Aldrich	Cat no.: T9284
Tween-20	Sigma Aldrich	Cat no.: 93773
S2 media	Gibco	Cat no.: 21720
FBS	Avantor	Cat no.: 97068-085
Penicillin-streptomycin	Gibco	Cat no.: 10378016
Paraformaldehyde	Sigma Aldrich	Cat no.: P6148
Bovine serum albumin	Sigma Aldrich	Cat no.: A2153
Hoechst	Thermo scientific	Cat no.: H1399
Glutaraldehyde	Sigma Aldrich	Cat no.: G7776
Osmium tetroxide	Sigma Aldrich	Cat no.: 75632
Propylene oxide	Sigma Aldrich	Cat no.: 110205
Embed-812	EMS	Cat no.: 14900
DER736	EMS	Cat no.: 13000
NMA	EMS	Cat no.: 19000
DMP-30	EMS	Cat no.: 13600
Uranyless	EMS	Cat no.: 22409
Super Signal West Pico Chemiluminescent Substrate	Thermo scientific	Cat no.: 34580
Resveratrol	Calbiochem	Cat no.: 554325
Oligonucleotides		
dAtg8aF: CGTCGCAAATATCCAGACCG dAtg8aR: GAAGAAGAGGGCATCCTCGG	IDT	NA

dAtg1F: GCCCAACGAACTGAAGTCCTA dAtg1R: TGGCATGTCAACTGGCGAC	IDT	NA
Ref(2)PF: TTCCAGGAGCGCCAGTTAC Ref(2)PR: CGTGCATATTGCTCTCGCAC	IDT	NA
ATPIF1F: CGTAGCGCATCTCGTCTGTA ATPIF1R: AGCTGCTCCCTTTGCTTCTT	IDT	NA
Hid F: GGTACATCCCAAGCGGAGAG Hid R: GGCCAAAACGAAAACGGTCA	IDT	NA
RP49 F: TCTGATGCCCAACATCGGTT RP49 R: TCTCCTTGCGCTTCTTGGAG	IDT	NA
Experimental models/Strains		
W^{1118}	BDSC	
$CG2135^{-/-}$	Bar *et al*., 2018	NA
Softwares		
Zen lite	Carl Zeiss	Version 3.4.91.00000
Fiji	Software	https://imagej.net/Fiji
Prism8	Software	https://www.graphpad.com/scientific-software/ prism/
LASx	Leica	

EXPERIMENTAL MODEL AND METHOD DETAILS:

Drosophila strains and maintenance

549 W^{1118} flies were obtained from the Bloomington *Drosophila* Stock Centre at Indiana University, USA.
550 The $CG2135^{-/-}$ fly used in this study was reported earlier from our lab by Bar *et. al.* [9] and was maintained
551 by routine outcrossing. W^{1118} and $CG2135^{-/-}$ flies were maintained in controlled density at 25°C under
552 a 12-hour day and night cycle. The standard cornmeal food (corn flour 75g/L, sugar 80g/L, agar 10g/L,
553 dry yeast 15g/L, and malt extract 30g/L) media was used for raising the flies.

554 For age-matched flies, flies were allowed to lay eggs after synchronization for 24 hours in a cage setup.
555 Then the freshly hatched larvae were collected in equal numbers in food vials. After 9-10 days the newly
556 eclosed flies were collected and used for respective in the experiments. For all the experiments only
557 male flies were used.

558 Resveratrol dissolved in 100% ethanol (Merck) was added to liquid cornmeal food at 400 µM
559 concentration as previously reported [9]. Flies were kept in continuous exposure of resveratrol starting at
560 day 4 after eclosion till the day of experiment. Resveratrol containing food vials were replaced with
561 fresh vials every alternative day.

562 **Starvation assay:**

563 Flies from W^{1118} and $CG2135^{-/-}$ of 4 days, 15 days, and 30 days old were assayed for their survivability
564 in no food condition. On the day of the experiment, flies in a cohort of 10 were kept in vials including
565 a tissue paper soaked in distilled water to mimic no food condition and maintained under a constant
566 temperature of 25°C with 12 hours dark and light cycle. The number of surviving flies monitored from
567 their mobility was considered alive or dead and recorded every 12 hours. More than 130 flies were
568 analysed for the starvation assay, and the experiment was done independently three times. The
569 percentage of survivability was calculated from the total number of flies and live flies at each time
570 point. To calculate mean survivability average number of flies that survived was determined [88].

571 **Western blot**

572 For western blot, 5-10 fly heads were homogenized in 1x Laemmli's (for 1ml 2X 0.5M Tris-Cl pH 6.8
573 0.312ml, SDS 0.05g, glycerol 0.25ml, 1M DTT 50µl) buffer supplemented with 1x protease inhibitor
574 cocktail and boiled at 100°C for 5 min. An equal volume of the fly lysate was subjected to SDS-PAGE.

575 Gels were transferred for 1 hour and blocked in 5% skim milk in 0.025% TBST. The primary antibody
576 incubation was done at 4°C overnight in respective dilutions of antibodies. The secondary antibodies
577 were incubated after washing for 1.5 hours. After final washing, the blots were developed using Super
578 Signal West Pico Chemiluminescent Substrate and captured using the ChemiDoc imaging system
579 (Biorad). α-Tubulin has been used as a loading control. Densitometric analysis of protein bands was
580 quantified using ImageJ software.

581 **Isolation of mitochondria-rich fraction from fly head**

582 Differential centrifugation was performed to isolate mitochondria from the fly head as described
583 previously [89]. Briefly, 50 fly heads were crushed gently with a mortar pestle (25 strokes) in 1 ml lysis
584 buffer containing 250 mM sucrose, 0.1 mM EDTA and 2 mM EGTA. Homogenate was centrifuged at
585 350g for 3 min to eliminate the tissue debris. The supernatant was centrifuged twice at 1000g to
586 eliminate the nuclear fraction. The mitochondria containing supernatant were centrifuged at 10000g for
587 10 min, the pellet was lysed in 1X Laemmeli's buffer and western blot was performed. All the steps
588 were performed in cold. Fractions were checked for the presence of mitochondrial and cytosolic proteins
589 determined by immunoblotting with ATP5A and GAPDH, respectively.

590 **RNA isolation and qRT-PCR**

591 Total RNA was isolated from 10-20 heads of W^{1118} and $CG2135^{-/-}$ flies using TRIzol reagent following
592 the manufacturer's instruction. 1 µg of RNA was used for DNase treatment and DNA-free RNA was
593 reverse transcribed using a cDNA synthesis kit. Transcript levels of different genes were quantified
594 using this cDNA as the template. Quantitative real-time PCR (qRT-PCR) was performed with SYBR
595 Green PCR reaction mix (BioRad) using the Biorad real-time PCR system. Target gene expression was
596 normalized to RP49 as the reference gene (endogenous control). The results of quantitative real-time
597 PCR were analysed by the comparative threshold cycle (CT) method [90].

598 **Immunostaining and imaging**

599 Adult brains from W^{1118} and $CG2135^{-/-}$ were dissected in S2 media supplemented with 10% FBS, 100
600 U/ml penicillin and 100 µg/ml streptomycin. The brains were fixed in 4% paraformaldehyde (PFA) for

601 30 minutes at room temperature. After fixation, the samples were washed in 0.3% PT (1x PBS + 0.3%
602 triton X-100) and blocked with PBT x GS (0.3% PT+0.5% BSA+ 5% Normal goat serum) for 2 hours.
603 The brains were incubated in primary antibodies at 4°C for 36 hours. Following incubation, the brains
604 were washed 5x with 0.3% PT for 15 minutes under gentle shaking conditions and incubated in
605 secondary antibody for 12 hours at 4°C. The washing steps were repeated and counter-stained with
606 DAPI (1μg/ml). After the final wash for 15 minutes the brains were stored in Vectashield until use in
607 the cold. The mounted brains were imaged in Apotome.2 microscope (Carl Zeiss) or Leica SP8 confocal
608 microscope. The image processing was done using the ZEN blue software from Carl Zeiss and for
609 quantification, ZEN blue software and ImageJ were used. For mean intensity measurement, 15-20
610 stacks from the Z planes were merged as MIP (maximum intensity projection) and the mean was taken
611 from the multiple ROIs for each field using ZEN blue.

612 **Mitotracker, Lysotracker, and JCI staining**

613 Mitotracker staining for age-matched flies was done after dissecting the brain in S2 media [9]. The
614 samples were incubated in 500 nM mitotracker for 1 hour and Hoechst (2μg/ml) with gentle shaking.
615 After incubation 2 quick washes were given with S2 media. The brains were mounted in media and
616 imaged immediately in Apotome.2 (Carl Zeiss). The intensity of the mitotracker per unit (1000 x 1000
617 pixel unit area) area and mitochondrial size were measured using ImageJ software.

618 For mitotracker and lysotracker co-staining, brains were dissected in S2 media. Following dissection
619 live brains were incubated with 500 nM mitotracker in S2 media for 30 minutes with Hoechst (2μg/ml)
620 hour at 25°C with gentle shaking in between. After 30 minutes, fresh Mitotracker along with 100 nM
621 lysotracker green and Hoechst was added and incubated for further 30 minutes. After incubation, 2
622 quick washes were given to remove the excess stain, followed by mounting in S2. The stained brains
623 were immediately imaged with Apotome.2 40X objective. Colocalization between mitotracker and
624 lysotracker was analysed using ImageJ. Single stacks of Z plane were taken and analysed using the
625 JaCoP plugin.

626 For JC1 staining the brains were dissected in S2 media supplemented with 10% FBS. Dissected brains
627 were incubated with 2 μM JC1 in S2+10% FBS for 45 mins. After incubation, the stain was discarded
628 and washed quickly with S2+10% FBS. Washed brains were mounted in S2+10% FBS and imaged
629 immediately using Apotome.2 (Carl Zeiss). The red-to-green ratio was calculated from individual stacks
630 analysed in ImageJ.

631 **TUNEL staining**

632 To determine the mechanism of cell death in W^{1118} and $CG2135^{-/-}$ TUNEL assay was performed [91]. The
633 brains were dissected in PBS and fixed in 4% PFA in 0.1% triton for 30mins. Then the samples were
634 washed 2 times each in 0.1% PT and 0.5% PT for 3 mins. The brains were permeabilized in sodium
635 citrate at 65°C for 30 minutes followed by three washes in 0.5% PT. The samples were incubated with
636 the TUNEL mix at 37°C for 3 hours following the manufacturer's instructions. After three washes with
637 0.1% PT and counter-staining with DAPI, the brains were stored in Vectashield and imaged the next
638 day in Apotome.2 (Carl Zeiss). Images acquired were processed in ZEN. 15-20 Z-stacks were taken for
639 MIP and after threshold set for the samples count of TUNEL positive puncta was determined using
640 ImageJ. The count has been represented per brain.

641 For co-staining with TH (tyrosine hydroxylase), the dissected brain was first immunostained with anti-
642 TH antibody following the above-mentioned methodology used for the TUNEL staining protocol. The
643 brains were mounted in Vectashield and imaged in 63x oil objective Leica SP8 confocal. TUNEL-
644 positive dopaminergic neurons were analysed and manually counted.

645 **Lipofuscin imaging**

646 Lipofuscin imaging was performed following previously described protocol [92]. Briefly, brains from age-
647 matched flies were dissected in cold phosphate buffer and kept on ice for 20 minutes. Then, they were
648 immediately imaged in Apotome.2 (Carl Zeiss) using the FITC channel (Autofluorescence). The images
649 were processed in ZEN blue. To count the number of autofluorescence bodies, MIP of 15 stacks was
650 taken and the threshold was kept the same for all the samples and analysed in ImageJ.

651 **Tissue preparation and Electron microscopy (TEM)**

Briefly, the dissected brains were fixed in 2.5% glutaraldehyde overnight, followed by post-fixation in 1% osmium tetroxide for 6h. The fixed tissues were dehydrated in a gradient of ethanol (30 to 100%) and finally in propylene oxide. Dehydrated tissues were infiltrated with resin (Embed-812 2ml, DER736 8ml, NMA 8.9ml and DMP-30 0.28ml) overnight. The next day, individual samples were embedded in capsule moulds and kept at 60°C for 48 hours to facilitate hardening. The samples were cut into ultra-thin using Leica Ultramicrotome. Sections of 70nm were negatively stained in uranyless. The images were acquired in Jeol JEM 2100Plus at 200 keV. The samples were analysed using ImageJ to determine the size and number of mitochondria and multilamellar bodies.

ATP quantification

Total ATP was quantified using an ATP determination kit. For each set of measurement, 10-15 fly heads were homogenized in 1X PBS supplemented with 1X PIC in cold. Supernatant collected by centrifuging the homogenate at 20000g for 20 min was used to measure ATP. Total ATP quantified following manufacturer protocol using a standard curve generated with known concentrations of ATP. Total ATP content was normalized per µg of total protein.

Statistical analysis

All the experiments were done at least three times independently. All statistical analysis were done using GraphPad Prism. p-values ≤ 0.05 were considered statistically significant as indicated by asterisks: $*P \leq 0.05$, $**P \leq 0.01$, and $***P \leq 0.001$.

References

1. Sly, W.S., Quinton, B.A., McAlister, W.H., and Rimoin, D.L. (1973). Beta glucuronidase deficiency: Report of clinical, radiologic, and biochemical features of a new mucopolysaccharidosis. J Pediatr *82*, 249–257. https://doi.org/10.1016/S0022-3476(73)80162-3.

2. Shipley, J.M., Klinkenberg, M., Wu, B.M., Bachinsky, D.R., Grubb, J.H., and Sly, W.S. (1993). Mutational analysis of a patient with mucopolysaccharidosis type VII, and identification of pseudogenes. Am J Hum Genet *52*, 517.

3. Montaño, A.M., Lock-Hock, N., Steiner, R.D., Graham, B.H., Szlago, M., Greenstein, R., Pineda, M., Gonzalez-Meneses, A., çoker, M., Bartholomew, D., et al. (2016). Clinical course of sly syndrome (mucopolysaccharidosis type VII). J Med Genet *53*, 403–418. https://doi.org/10.1136/JMEDGENET-2015-103322.

4. Wallace, S.P., Prutting, C.A., and Gerber, S.E. (1990). Degeneration of speech, language, and hearing in a patient with mucopolysaccharidosis VII. Int J Pediatr Otorhinolaryngol *19*, 97–107. https://doi.org/10.1016/0165-5876(90)90215-D.

5. Vogler, C., Levy, B., Kyle, J.W., Sly, W., Williamson, J., and Whyte, M. (1994). Mucopolysaccharidosis VII: postmortem biochemical and pathological findings in a young adult with beta-glucuronidase deficiency. Modern Pathology.

6. Levy, B., Galvin, N., Vogler, C., Birkenmeier, E.H., and Sly, W.S. (1996). Neuropathology of murine mucopolysaccharidosis type VII. Acta Neuropathol *92*, 562–568. https://doi.org/10.1007/S004010050562/METRICS.

7. Harmatz, P., Whitley, C.B., Wang, R.Y., Bauer, M., Song, W., Haller, C., and Kakkis, E. (2018). A novel Blind Start study design to investigate vestronidase alfa for mucopolysaccharidosis VII, an ultra-rare genetic disease. Mol Genet Metab *123*, 488–494. https://doi.org/10.1016/J.YMGME.2018.02.006.

8. Wang, R.Y., da Silva Franco, J.F., López-Valdez, J., Martins, E., Sutton, V.R., Whitley, C.B., Zhang, L., Cimms, T., Marsden, D., Jurecka, A., et al. (2020). The long-term safety and efficacy of vestronidase alfa, rhGUS enzyme replacement therapy, in subjects with mucopolysaccharidosis VII. Mol Genet Metab *129*, 219–227. https://doi.org/10.1016/J.YMGME.2020.01.003.

9. Bar, S., Prasad, M., and Datta, R. (2018). Neuromuscular degeneration and locomotor deficit in a Drosophila model of mucopolysaccharidosis VII is attenuated by treatment with resveratrol. Dis Model Mech *11*. https://doi.org/10.1242/DMM.036954.

10. Zhou, Q.Y., and Palmiter, R.D. (1995). Dopamine-deficient mice are severely hypoactive, adipsic, and aphagic. Cell *83*, 1197–1209. https://doi.org/10.1016/0092-8674(95)90145-0.

11. Auluck, P.K., Chan, H.Y.E., Trojanowski, J.Q., Lee, V.M.Y., and Bonini, N.M. (2002). Chaperone suppression of α-synuclein toxicity in a Drosophila model for Parkinson's disease. Science (1979) *295*, 865–868. https://doi.org/10.1126/SCIENCE.1067389/SUPPL_FILE/1067389S1_THUMB.GIF.

12. Martins, C., Hulkova, H., Dridi, L., Dormoy-Raclet, V., Grigoryeva, L., Choi, Y., Langford-Smith, A., Wilkinson, F.L., Ohmi, K., DiCristo, G., et al. (2015). Neuroinflammation, mitochondrial defects and neurodegeneration in mucopolysaccharidosis III type C mouse model. Brain *138*, 336. https://doi.org/10.1093/BRAIN/AWU355.

13. Kinghorn, K.J., Grönke, S., Castillo-Quan, J.I., Woodling, N.S., Li, L., Sirka, E., Gegg, M., Mills, K., Hardy, J., Bjedov, I., et al. (2016). A Drosophila Model of Neuronopathic Gaucher Disease Demonstrates Lysosomal-Autophagic Defects and Altered mTOR Signalling and Is Functionally Rescued by Rapamycin. The Journal of Neuroscience *36*, 11654. https://doi.org/10.1523/JNEUROSCI.4527-15.2016.

14. Settembre, C., Fraldi, A., Jahreiss, L., Spampanato, C., Venturi, C., Medina, D., de Pablo, R., Tacchetti, C., Rubinsztein, D.C., and Ballabio, A. (2008). A block of autophagy in lysosomal storage disorders. Hum Mol Genet *17*, 119–129. https://doi.org/10.1093/HMG/DDM289.

15. Lopez-Fabuel, I., Garcia-Macia, M., Buondelmonte, C., Burmistrova, O., Bonora, N., Alonso-Batan, P., Morant-Ferrando, B., Vicente-Gutierrez, C., Jimenez-Blasco, D., Quintana-Cabrera, R., et al. (2022). Aberrant upregulation of the glycolytic enzyme PFKFB3 in CLN7 neuronal ceroid lipofuscinosis. Nat Commun *13*. https://doi.org/10.1038/S41467-022-28191-1.

16. Rugarli, E.I., and Langer, T. (2012). Mitochondrial quality control: A matter of life and death for neurons. EMBO Journal *31*, 1336–1349. https://doi.org/10.1038/EMBOJ.2012.38/ASSET/B98C1CBF-817A-412A-A7BF-0E97278DF16A/ASSETS/GRAPHIC/EMBJ201238-FIG-0004-M.JPG.

17. Seo, A.Y., Joseph, A.M., Dutta, D., Hwang, J.C.Y., Aris, J.P., and Leeuwenburgh, C. (2010). New insights into the role of mitochondria in aging: mitochondrial dynamics and more. J Cell Sci *123*, 2533–2542. https://doi.org/10.1242/JCS.070490.

18. Wang, Y., Liu, N., and Lu, B. (2019). Mechanisms and roles of mitophagy in neurodegenerative diseases. CNS Neurosci Ther *25*, 859. https://doi.org/10.1111/CNS.13140.

19. Basu, I., Bar, S., Prasad, M., and Datta, R. (2022). Adipose deficiency and aberrant autophagy in a Drosophila model of MPS VII is corrected by pharmacological stimulators of mTOR. Biochim Biophys Acta Mol Basis Dis *1868*. https://doi.org/10.1016/J.BBADIS.2022.166399.

20. Bartolomeo, R., Cinque, L., De Leonibus, C., Forrester, A., Salzano, A.C., Monfregola, J., De Gennaro, E., Nusco, E., Azario, I., Lanzara, C., et al. (2017). mTORC1 hyperactivation arrests bone growth in lysosomal storage disorders by suppressing autophagy. J Clin Invest *127*, 3717–3729. https://doi.org/10.1172/JCI94130.

21. Morishita, H., and Mizushima, N. (2019). Diverse cellular roles of autophagy. Annu Rev Cell Dev Biol *35*, 453–475. https://doi.org/10.1146/ANNUREV-CELLBIO-100818-125300/CITE/REFWORKS.

22. Mizushima, N., Yoshimori, T., and Ohsumi, Y. (2011). The role of Atg proteins in autophagosome formation. Annu Rev Cell Dev Biol *27*, 107–132. https://doi.org/10.1146/ANNUREV-CELLBIO-092910-154005.

23. Mochida, K., and Nakatogawa, H. (2022). ER -phagy: selective autophagy of the endoplasmic reticulum . EMBO Rep *23*. https://doi.org/10.15252/EMBR.202255192/ASSET/5503D294-66FB-40A0-B536-6AD10D176ED0/ASSETS/GRAPHIC/EMBR202255192-FIG-0004-M.PNG.

24. Shang, L., Chen, S., Du, F., Li, S., Zhao, L., and Wang, X. (2011). Nutrient starvation elicits an acute autophagic response mediated by Ulk1 dephosphorylation and its subsequent dissociation from AMPK. Proc Natl Acad Sci U S A *108*, 4788–4793. https://doi.org/10.1073/PNAS.1100844108/-/DCSUPPLEMENTAL/PNAS.1100844108_SI.PDF.

25. Scott, R.C., Schuldiner, O., and Neufeld, T.P. (2004). Role and regulation of starvation-induced autophagy in the Drosophila fat body. Dev Cell *7*, 167–178. https://doi.org/10.1016/J.DEVCEL.2004.07.009.

26. Komatsu, M., Waguri, S., Ueno, T., Iwata, J., Murata, S., Tanida, I., Ezaki, J., Mizushima, N., Ohsumi, Y., Uchiyama, Y., et al. (2005). Impairment of starvation-induced and constitutive autophagy in Atg7-deficient mice. Journal of Cell Biology *169*, 425–434. https://doi.org/10.1083/JCB.200412022.

27. Kang, C., You, N.J., and Avery, L. (2007). Dual roles of autophagy in the survival of Caenorhabditis elegans during starvation. Genes Dev *21*, 2161. https://doi.org/10.1101/GAD.1573107.

28. Mizushima, N., and Yoshimori, T. (2007). How to Interpret LC3 Immunoblotting. Autophagy *3*, 542–545. https://doi.org/10.4161/AUTO.4600.

29. Nezis, I.P., Simonsen, A., Sagona, A.P., Finley, K., Gaumer, S., Contamine, D., Rusten, T.E., Stenmark, H., and Brech, A. (2008). Ref(2)P, the Drosophila melanogaster homologue of mammalian p62, is required for the formation of protein aggregates in adult brain. J Cell Biol *180*, 1065. https://doi.org/10.1083/JCB.200711108.

30. Hurley, J.H., and Young, L.N. (2017). Mechanisms of autophagy initiation. Annu Rev Biochem *86*, 225–244. https://doi.org/10.1146/ANNUREV-BIOCHEM-061516-044820/CITE/REFWORKS.

31. Terman, A., and Brunk, U.T. (2004). Lipofuscin. Int J Biochem Cell Biol *36*, 1400–1404. https://doi.org/10.1016/J.BIOCEL.2003.08.009.

32. Haltia, M. (2003). The neuronal ceroid-lipofuscinoses. J Neuropathol Exp Neurol *62*, 1–13. https://doi.org/10.1093/JNEN/62.1.1.

33. Venkatachalam, K., Long, A.A., Elsaesser, R., Nikolaeva, D., Broadie, K., and Montell, C. (2008). Motor deficit in a Drosophila model of mucolipidosis type IV due to defective clearance of apoptotic cells. Cell *135*, 838–851. https://doi.org/10.1016/J.CELL.2008.09.041.

34. Pan, C., Banerjee, K., Lehmann, G.L., Almeida, D., Hajjar, K.A., Benedicto, I., Jiang, Z., Radu, R.A., Thompson, D.H., Rodriguez-Boulan, E., et al. (2021). Lipofuscin causes atypical necroptosis through lysosomal membrane permeabilization. Proc Natl Acad Sci U S A *118*, e2100122118. https://doi.org/10.1073/PNAS.2100122118/SUPPL_FILE/PNAS.2100122118.SAPP.PDF.

35. Hariri, M., Millane, G., Guimond, M.P., Guay, G., Dennis, J.W., and Nabi, I.R. (2000). Biogenesis of Multilamellar Bodies via Autophagy. Mol Biol Cell *11*, 255. https://doi.org/10.1091/MBC.11.1.255.

36. Cunningham, K.M., Maulding, K., Ruan, K., Senturk, M., Grima, J.C., Sung, H., Zuo, Z., Song, H., Gao, J., Dubey, S., et al. (2020). Tfeb/mitf links impaired nuclear import to autophagolysosomal dysfunction in c9-als. Elife *9*, 1–35. https://doi.org/10.7554/ELIFE.59419.

37. Brandt, T., Mourier, A., Tain, L.S., Partridge, L., Larsson, N.G., and Kühlbrandt, W. (2017). Changes of mitochondrial ultrastructure and function during ageing in mice and Drosophila. Elife *6*. https://doi.org/10.7554/ELIFE.24662.

38. Lou, G., Palikaras, K., Lautrup, S., Scheibye-Knudsen, M., Tavernarakis, N., and Fang, E.F. (2020). Mitophagy and Neuroprotection. Trends Mol Med *26*, 8–20. https://doi.org/10.1016/J.MOLMED.2019.07.002.

39. Han, S., Zhang, M., Jeong, Y.Y., Margolis, D.J., and Cai, Q. (2021). The role of mitophagy in the regulation of mitochondrial energetic status in neurons. Autophagy *17*, 4182. https://doi.org/10.1080/15548627.2021.1907167.

40. Zorova, L.D., Popkov, V.A., Plotnikov, E.Y., Silachev, D.N., Pevzner, I.B., Jankauskas, S.S., Babenko, V.A., Zorov, S.D., Balakireva, A. V., Juhaszova, M., et al. (2018). Mitochondrial membrane potential. Anal Biochem *552*, 50–59. https://doi.org/10.1016/J.AB.2017.07.009.

41. Gledhill, J.R., Montgomery, M.G., Leslie, A.G.W., and Walker, J.E. (2007). How the regulatory protein, IF(1), inhibits F(1)-ATPase from bovine mitochondria. Proc Natl Acad Sci U S A *104*, 15671–15676. https://doi.org/10.1073/PNAS.0707326104.

42. Li, S., Zhang, J., Liu, C., Wang, Q., Yan, J., Hui, L., Jia, Q., Shan, H., Tao, L., and Zhang, M. (2021). The Role of Mitophagy in Regulating Cell Death. Oxid Med Cell Longev *2021*. https://doi.org/10.1155/2021/6617256.

43. Pathak, D., Berthet, A., and Nakamura, K. (2013). Energy Failure: Does It Contribute to Neurodegeneration? Ann Neurol *74*, 506. https://doi.org/10.1002/ANA.24014.

44. Lieberthal, W., Menza, S.A., and Levine, J.S. (1998). Graded ATP depletion can cause necrosis or apoptosis of cultured mouse proximal tubular cells. Am J Physiol *274*. https://doi.org/10.1152/AJPRENAL.1998.274.2.F315.

45. Porter, A.G., and Jänicke, R.U. (1999). Emerging roles of caspase-3 in apoptosis. Cell Death Differ *6*, 99–104. https://doi.org/10.1038/SJ.CDD.4400476.

46. Koushika, S.P., Lisbin, M.J., and White, K. (1996). ELAV, a Drosophila neuron-specific protein, mediates the generation of an alternatively spliced neural protein isoform. Curr Biol *6*, 1634–1641. https://doi.org/10.1016/S0960-9822(02)70787-2.

47. Goyal, L., McCall, K., Agapite, J., Hartwieg, E., and Steller, H. (2000). Induction of apoptosis by Drosophila reaper, hid and grim through inhibition of IAP function. EMBO J *19*, 589. https://doi.org/10.1093/EMBOJ/19.4.589.

48. Menzies, F.M., Fleming, A., Caricasole, A., Bento, C.F., Andrews, S.P., Ashkenazi, A., Füllgrabe, J., Jackson, A., Jimenez Sanchez, M., Karabiyik, C., et al. (2017). Autophagy and Neurodegeneration: Pathogenic Mechanisms and Therapeutic Opportunities. Neuron *93*, 1015–1034. https://doi.org/10.1016/J.NEURON.2017.01.022.

49. Mizushima, N., Yamamoto, A., Matsui, M., Yoshimori, T., and Ohsumi, Y. (2004). In vivo analysis of autophagy in response to nutrient starvation using transgenic mice expressing a fluorescent autophagosome marker. Mol Biol Cell *15*, 1101–1111. https://doi.org/10.1091/MBC.E03-09-0704.

50. Rubinsztein, D.C., Mariño, G., and Kroemer, G. (2011). Autophagy and aging. Cell *146*, 682–695. https://doi.org/10.1016/J.CELL.2011.07.030.

51. Chang, J.T., Kumsta, C., Hellman, A.B., Adams, L.M., and Hansen, M. (2017). Spatiotemporal regulation of autophagy during Caenorhabditis elegans aging. Elife *6*. https://doi.org/10.7554/ELIFE.18459.

52. Schreiber, A., Collins, B.C., Davis, C., Enchev, R.I., Sedra, A., D'Antuono, R., Aebersold, R., and Peter, M. (2021). Multilayered regulation of autophagy by the Atg1 kinase orchestrates spatial and temporal control of autophagosome formation. Mol Cell *81*, 5066-5081.e10. https://doi.org/10.1016/J.MOLCEL.2021.10.024.

53. Zou, L., Liao, M., Zhen, Y., Zhu, S., Chen, X., Zhang, J., Hao, Y., and Liu, B. (2022). Autophagy and beyond: Unraveling the complexity of UNC-51-like kinase 1 (ULK1) from biological functions to therapeutic implications. Acta Pharm Sin B *12*, 3743–3782. https://doi.org/10.1016/J.APSB.2022.06.004.

54. Kim, J., Kundu, M., Viollet, B., and Guan, K.L. (2011). AMPK and mTOR regulate autophagy through direct phosphorylation of Ulk1. Nature Cell Biology 2011 13:2 *13*, 132–141. https://doi.org/10.1038/ncb2152.

55. Sánchez-Martın, P., and Komatsu, M. (2018). p62/SQSTM1 - steering the cell through health and disease. J Cell Sci *131*. https://doi.org/10.1242/JCS.222836.

56. Ivanova, M.M., Changsila, E., Iaonou, C., and Goker-Alpan, O. (2019). Impaired autophagic and mitochondrial functions are partially restored by ERT in Gaucher and Fabry diseases. PLoS One *14*. https://doi.org/10.1371/JOURNAL.PONE.0210617.

57. Settembre, C., Di Malta, C., Polito, V.A., Arencibia, M.G., Vetrini, F., Erdin, S., Erdin, S.U., Huynh, T., Medina, D., Colella, P., et al. (2011). TFEB links autophagy to lysosomal biogenesis. Science *332*, 1429–1433. https://doi.org/10.1126/SCIENCE.1204592.

58. Cortes, C.J., and La Spada, A.R. (2019). TFEB dysregulation as a driver of autophagy dysfunction in neurodegenerative disease: Molecular mechanisms, cellular processes, and emerging therapeutic opportunities. Neurobiol Dis *122*, 83–93. https://doi.org/10.1016/J.NBD.2018.05.012.

59. Toro, C., Zainab, M., and Tifft, C.J. (2021). The GM2 gangliosidoses: Unlocking the mysteries of pathogenesis and treatment. Neurosci Lett *764*. https://doi.org/10.1016/J.NEULET.2021.136195.

60. Oldfors, A., and Sourander, P. (1981). Storage of lipofuscin in neurons in mucopolysaccharidosis - Report on a case of Sanfilippo's syndrome with histochemical and electron-microscopic findings. Acta Neuropathol *54*, 287–292. https://doi.org/10.1007/BF00697002/METRICS.

61. García-Sanz, P., Orgaz, L., Bueno-Gil, G., Espadas, I., Rodríguez-Traver, E., Kulisevsky, J., Gutierrez, A., Dávila, J.C., González-Polo, R.A., Fuentes, J.M., et al. (2017). N370S-GBA1 mutation causes lysosomal cholesterol accumulation in Parkinson's disease. Movement Disorders *32*, 1409–1422. https://doi.org/10.1002/MDS.27119.

62. Komatsu, M., Waguri, S., Chiba, T., Murata, S., Iwata, J.I., Tanida, I., Ueno, T., Koike, M., Uchiyama, Y., Kominami, E., et al. (2006). Loss of autophagy in the central nervous system causes neurodegeneration in mice. Nature 2006 441:7095 *441*, 880–884. https://doi.org/10.1038/nature04723.

63. Choi, I., Wang, M., Yoo, S., Xu, P., Seegobin, S.P., Li, X., Han, X., Wang, Q., Peng, J., Zhang, B., et al. (2023). Autophagy enables microglia to engage amyloid plaques and prevents microglial senescence. Nature Cell Biology 2023 25:7 *25*, 963–974. https://doi.org/10.1038/s41556-023-01158-0.

64. Nixon, R.A., and Rubinsztein, D.C. (2024). Mechanisms of autophagy–lysosome dysfunction in neurodegenerative diseases. Nature Reviews Molecular Cell Biology 2024, 1–21. https://doi.org/10.1038/s41580-024-00757-5.

65. Padamsey, Z., and Rochefort, N.L. (2023). Paying the brain's energy bill. Curr Opin Neurobiol *78*, 102668. https://doi.org/10.1016/J.CONB.2022.102668.

66. Palikaras, K., Lionaki, E., and Tavernarakis, N. (2018). Mechanisms of mitophagy in cellular homeostasis, physiology and pathology. Nature Cell Biology 2018 20:9 *20*, 1013–1022. https://doi.org/10.1038/s41556-018-0176-2.

67. Ham, S.J., Lee, D., Xu, W.J., Cho, E., Choi, S., Min, S., Park, S., and Chung, J. (2021). Loss of UCHL1 rescues the defects related to Parkinson's disease by suppressing glycolysis. Sci Adv *7*. https://doi.org/10.1126/SCIADV.ABG4574/SUPPL_FILE/ABG4574_SM.PDF.

68. Egan, D.F., Shackelford, D.B., Mihaylova, M.M., Gelino, S., Kohnz, R.A., Mair, W., Vasquez, D.S., Joshi, A., Gwinn, D.M., Taylor, R., et al. (2011). Phosphorylation of ULK1 (hATG1) by AMP-activated protein kinase connects energy sensing to mitophagy. Science *331*, 456. https://doi.org/10.1126/SCIENCE.1196371.

69. Hung, C.M., Lombardo, P.S., Malik, N., Brun, S.N., Hellberg, K., Van Nostrand, J.L., Garcia, D., Baumgart, J., Diffenderfer, K., Asara, J.M., et al. (2021). AMPK/ULK1-mediated phosphorylation of Parkin ACT domain mediates an early step in mitophagy. Sci Adv *7*. https://doi.org/10.1126/SCIADV.ABG4544.

70. Wu, W., Tian, W., Hu, Z., Chen, G., Huang, L., Li, W., Zhang, X., Xue, P., Zhou, C., Liu, L., et al. (2014). ULK1 translocates to mitochondria and phosphorylates FUNDC1 to regulate mitophagy. EMBO Rep *15*, 566. https://doi.org/10.1002/EMBR.201438501.

71. Chen, S., Zhou, L., Zhang, Y., Leng, Y., Pei, X.-Y., Lin, H., Jones, R., Orlowski, R.Z., Dai, Y., and Grant, S. (2014). Targeting SQSTM1/p62 induces cargo loading failure and converts autophagy to apoptosis via NBK/Bik. Mol Cell Biol *34*, 3435–3449. https://doi.org/10.1128/MCB.01383-13.

72. Geisler, S., Holmström, K.M., Skujat, D., Fiesel, F.C., Rothfuss, O.C., Kahle, P.J., and Springer, W. (2010). PINK1/Parkin-mediated mitophagy is dependent on VDAC1 and p62/SQSTM1. Nat Cell Biol *12*, 119–131. https://doi.org/10.1038/NCB2012.

73. Chen, Y., and Dorn, G.W. (2013). PINK1- Phosphorylated Mitofusin 2 is a Parkin Receptor for Culling Damaged Mitochondria. Science *340*, 471. https://doi.org/10.1126/SCIENCE.1231031.

74. Hwang, S., Disatnik, M.-H., and Mochly-Rosen, D. (2015). Impaired GAPDH-induced mitophagy contributes to the pathology of Huntington's disease. EMBO Mol Med *7*, 1307. https://doi.org/10.15252/EMMM.201505256.

75. Yu, W., Gong, J.S., Ko, M., Garver, W.S., Yanagisawa, K., and Michikawa, M. (2005). Altered cholesterol metabolism in Niemann-Pick type C1 mouse brains affects mitochondrial function. J Biol Chem *280*, 11731–11739. https://doi.org/10.1074/JBC.M412898200.

76. Bosch, M.E., and Kielian, T. (2019). Astrocytes in juvenile neuronal ceroid lipofuscinosis (CLN3) display metabolic and calcium signaling abnormalities. J Neurochem *148*, 612–624. https://doi.org/10.1111/JNC.14545.

77. Feldenberg, L.R., Thevananther, S., Del Rio, M., De Leon, M., and Devarajan, P. (1999). Partial ATP depletion induces Fas- and caspase-mediated apoptosis in MDCK cells. Am J Physiol Renal Physiol *276*. https://doi.org/10.1152/AJPRENAL.1999.276.6.F837/ASSET/IMAGES/LARGE/AFLU20602007W.JPEG.

78. Levine, B., and Kroemer, G. (2008). Autophagy in the Pathogenesis of Disease. Cell *132*, 27. https://doi.org/10.1016/J.CELL.2007.12.018.

79. Ravikumar, B., Vacher, C., Berger, Z., Davies, J.E., Luo, S., Oroz, L.G., Scaravilli, F., Easton, D.F., Duden, R., and O'kane, C.J. (2006). Rapamycin pre-treatment protects against apoptosis. Hum Mol Genet *15*, 1209–1216. https://doi.org/10.1093/HMG/DDL036.

80. Boya, P., González-Polo, R.-A., Casares, N., Perfettini, J.-L., Dessen, P., Larochette, N., Métivier, D., Meley, D., Souquere, S., Yoshimori, T., et al. (2005). Inhibition of macroautophagy triggers apoptosis. Mol Cell Biol *25*, 1025–1040. https://doi.org/10.1128/MCB.25.3.1025-1040.2005.

81. Venderova, K., and Park, D.S. (2012). Programmed Cell Death in Parkinson's Disease. Cold Spring Harb Perspect Med *2*. https://doi.org/10.1101/CSHPERSPECT.A009365.

82. Surmeier, D.J., Obeso, J.A., and Halliday, G.M. (2017). Selective neuronal vulnerability in Parkinson disease. Nat Rev Neurosci *18*, 101–113. https://doi.org/10.1038/NRN.2016.178.

83. Lin, K.L., Lin, K.J., Wang, P.W., Chuang, J.H., Lin, H.Y., Chen, S. Der, Chuang, Y.C., Huang, S.T., Tiao, M.M., Chen, J.B., et al. (2018). Resveratrol provides neuroprotective effects through modulation of mitochondrial dynamics and ERK1/2 regulated autophagy. Free Radic Res *52*, 1371–1386. https://doi.org/10.1080/10715762.2018.1489128.

84. Stork, T., Bernardos, R., and Freeman, M.R. (2012). Analysis of Glial Cell Development and Function in Drosophila. Cold Spring Harb Protoc *2012*, 1. https://doi.org/10.1101/PDB.TOP067587.

85. Zalfa, C., Verpelli, C., D'avanzo, F., Tomanin, R., Vicidomini, C., Cajola, L., Manara, R., Sala, C., Scarpa, M., Vescovi, A.L., et al. (2016). Glial degeneration with oxidative damage drives neuronal demise in MPSII disease. Cell Death Dis *7*, e2331. https://doi.org/10.1038/CDDIS.2016.231.

86. Morales, I., Sanchez, A., Puertas-Avendaño, R., Rodriguez-Sabate, C., Perez-Barreto, A., and Rodriguez, M. (2020). Neuroglial transmitophagy and Parkinson's disease. Glia *68*, 2277–2299. https://doi.org/10.1002/GLIA.23839.

87. Lautrup, S., Lou, G., Aman, Y., Nilsen, H., Tao, J., and Fang, E.F. (2019). Microglial mitophagy mitigates neuroinflammation in Alzheimer's disease. Neurochem Int *129*, 104469. https://doi.org/10.1016/J.NEUINT.2019.104469.

88. Lushchak, O. V., Gospodaryov, D. V., Rovenko, B.M., Glovyak, A.D., Yurkevych, I.S., Klyuba, V.P., Shcherbij, M. V., and Lushchak, V.I. (2012). Balance between macronutrients affects life span and functional senescence in fruit fly Drosophila melanogaster. J Gerontol A Biol Sci Med Sci *67*, 118–125. https://doi.org/10.1093/GERONA/GLR184.

89. Rana, A., Oliveira, M.P., Khamoui, A. V., Aparicio, R., Rera, M., Rossiter, H.B., and Walker, D.W. (2017). Promoting Drp1-mediated mitochondrial fission in midlife prolongs healthy lifespan of Drosophila melanogaster. Nat Commun *8*. https://doi.org/10.1038/S41467-017-00525-4.

90. Livak, K.J., and Schmittgen, T.D. (2001). Analysis of relative gene expression data using real-time quantitative PCR and the 2(-Delta Delta C(T)) Method. Methods *25*, 402–408. https://doi.org/10.1006/METH.2001.1262.

91. Denton, D., Mills, K., and Kumar, S. (2008). Methods and protocols for studying cell death in Drosophila. Methods Enzymol *446*, 17–37. https://doi.org/10.1016/S0076-6879(08)01602-9.

92. Hebbar, S., Khandelwal, A., Jayashree, R., Hindle, S.J., Chiang, Y.N., Yew, J.Y., Sweeney, S.T., and Schwudke, D. (2017). Lipid metabolic perturbation is an early-onset phenotype in adult spinster mutants: a Drosophila model for lysosomal storage disorders. Mol Biol Cell *28*, 3728–3740. https://doi.org/10.1091/MBC.E16-09-0674.

Figure 1

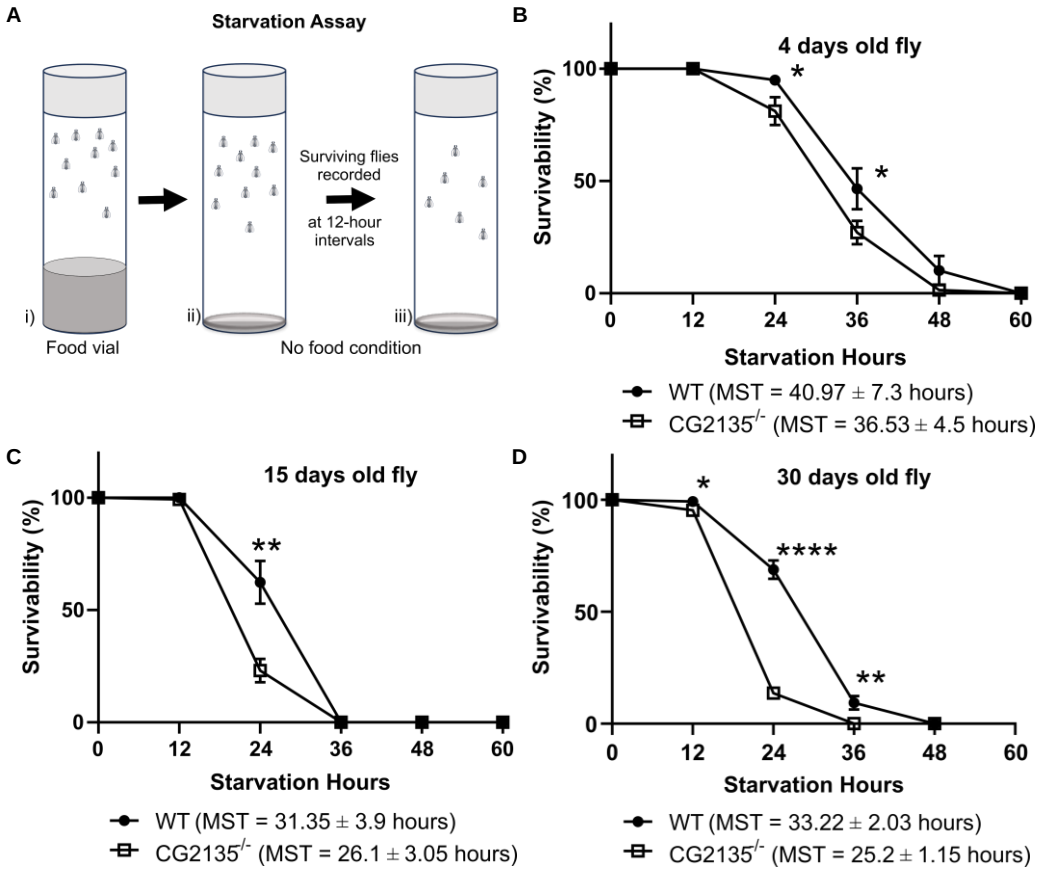
A
Starvation Assay
Surviving flies recorded
at 12-hour intervals
i)
Food vial
ii)
iii)
No food condition
B
4 days old fly
Survivability (%)
Starvation Hours
WT (MST = 40.97 ± 7.3 hours)
CG2135-/- (MST = 36.53 ± 4.5 hours)
C
15 days old fly
Survivability (%)
Starvation Hours
WT (MST = 31.35 ± 3.9 hours)
CG2135-/- (MST = 26.1 ± 3.05 hours)
D
30 days old fly
Survivability (%)
Starvation Hours
WT (MST = 33.22 ± 2.03 hours)
CG2135-/- (MST = 25.2 ± 1.15 hours)

Figure 2

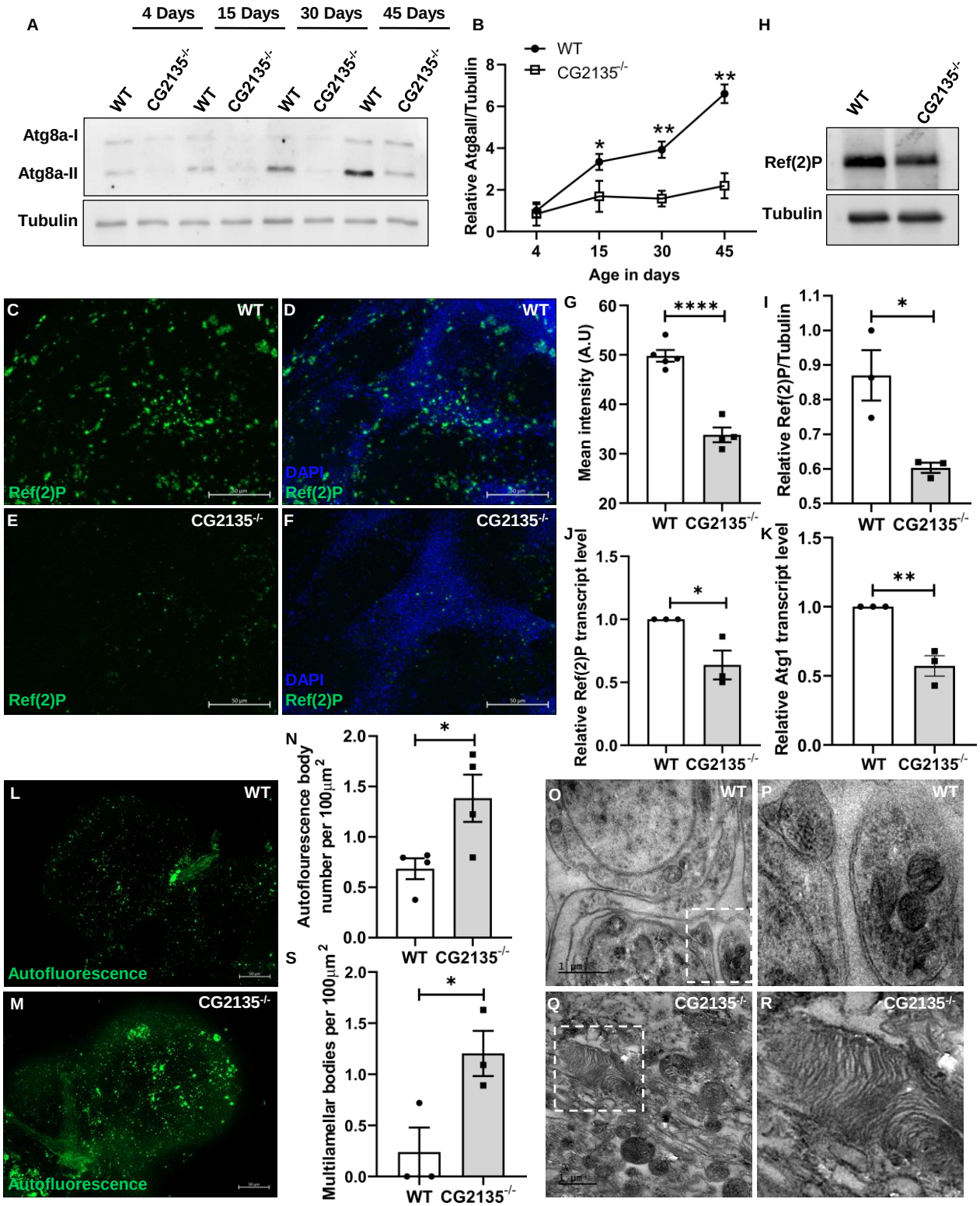
A
4 Days
15 Days
30 Days
45 Days
WT
CG2135-/-
Atg8a-I
Atg8a-II
Tubulin
B
WT
CG2135-/-
Relative Atg8aII/Tubulin
Age in days
H
Ref(2)P
Tubulin
C
D
E
F
Ref(2)P
DAPI
G
Mean intensity (A.U)
I
Relative Ref(2)P/Tubulin
J
Relative Ref(2)P transcript level
K
Relative Atg1 transcript level
L
M
Autofluorescence
N
Autoflourescence body number per 100μm2
S
Multilamellar bodies per 100μm2
O
P
Q
R

Figure 3

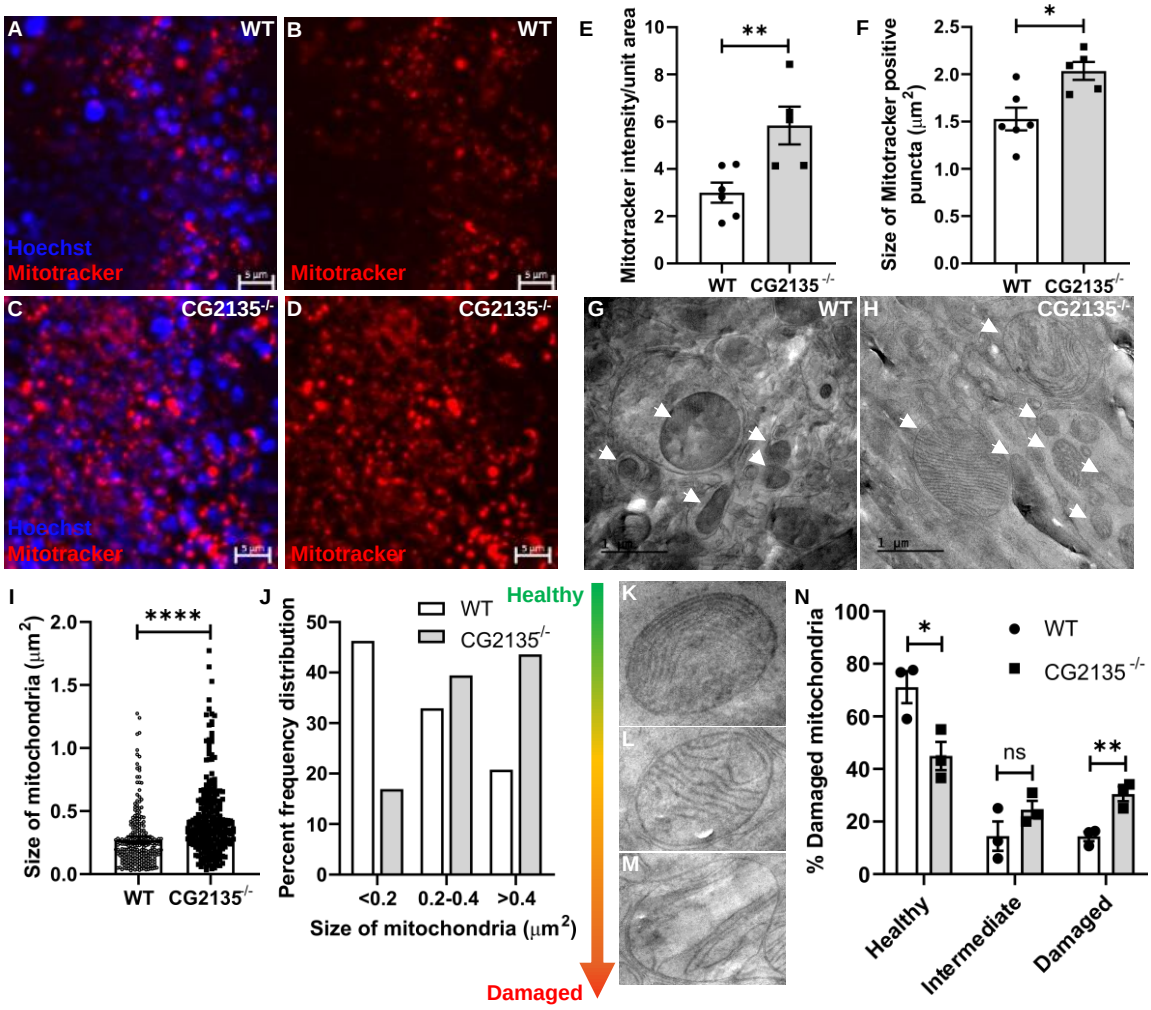
A
WT
Hoechst
Mitotracker
B
WT
Mitotracker
C
CG2135-/-
Hoechst
Mitotracker
D
CG2135-/-
Mitotracker
E
Mitotracker intensity/unit area
**
WT
CG2135 -/-
F
Size of Mitotracker positive puncta (μm2)
*
WT
CG2135-/-
G
WT
H
CG2135-/-
I
Size of mitochondria (μm2)
****
WT
CG2135-/-
J
Percent frequency distribution
WT
CG2135-/-
<0.2
0.2-0.4
>0.4
Size of mitochondria (μm2)
Healthy
Damaged
K
L
M
N
% Damaged mitochondria
WT
CG2135 -/-
*
ns
**
Healthy
Intermediate
Damaged

Figure 4

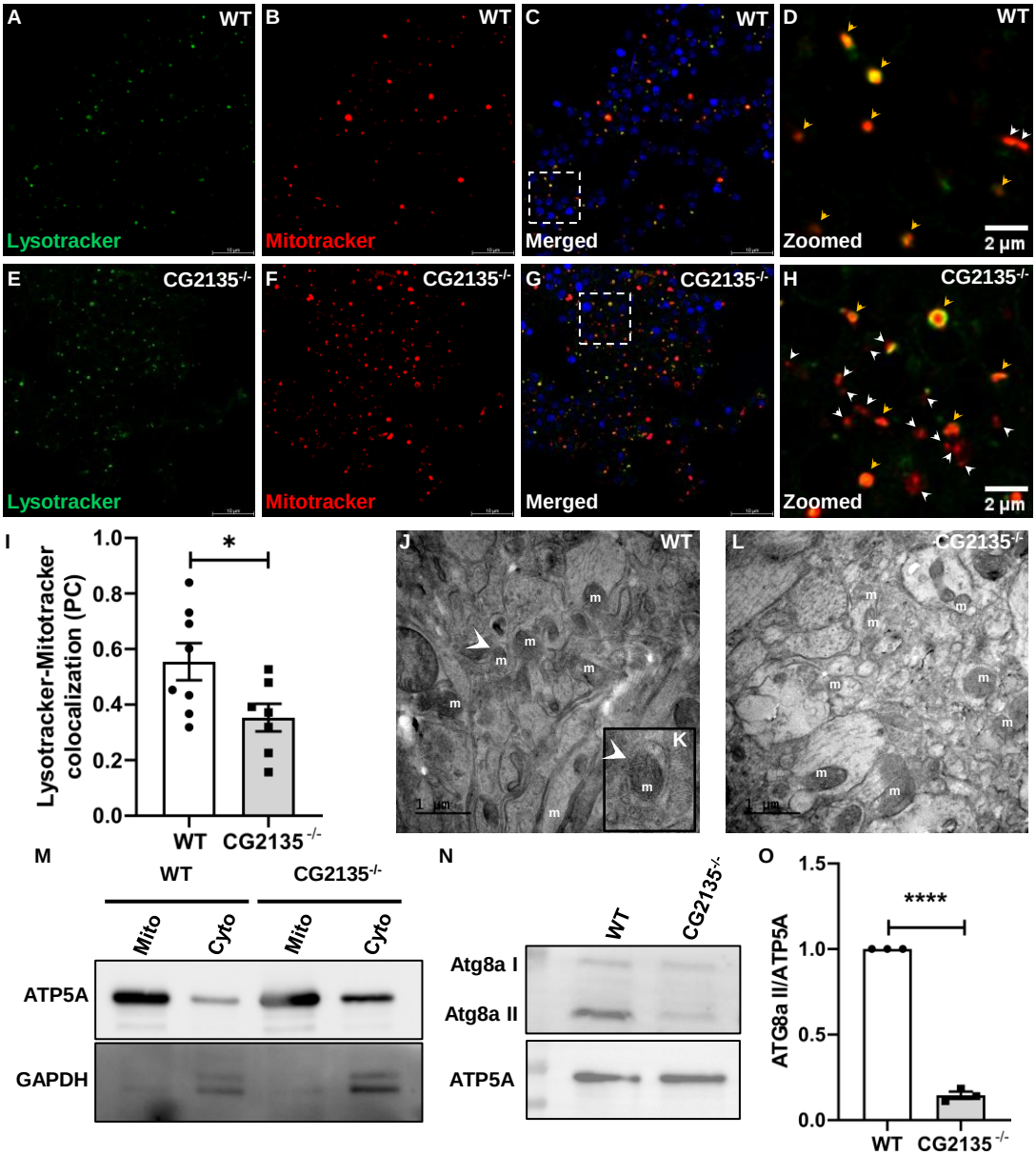
A
WT
Lysotracker
B
WT
Mitotracker
C
WT
Merged
D
WT
Zoomed
2 µm
E
CG2135-/-
Lysotracker
F
CG2135-/-
Mitotracker
G
CG2135-/-
Merged
H
CG2135-/-
Zoomed
2 µm
I
Lysotracker-Mitotracker colocalization (PC)
1.0
0.8
0.6
0.4
0.2
0.0
*
WT
CG2135 -/-
J
WT
K
m
1 µm
L
CG2135-/-
1 µm
M
WT
CG2135-/-
Mito
Cyto
Mito
Cyto
ATP5A
GAPDH
N
WT
CG2135-/-
Atg8a I
Atg8a II
ATP5A
O
ATG8a II/ATP5A
1.5
1.0
0.5
0.0
****
WT
CG2135 -/-

Figure 5

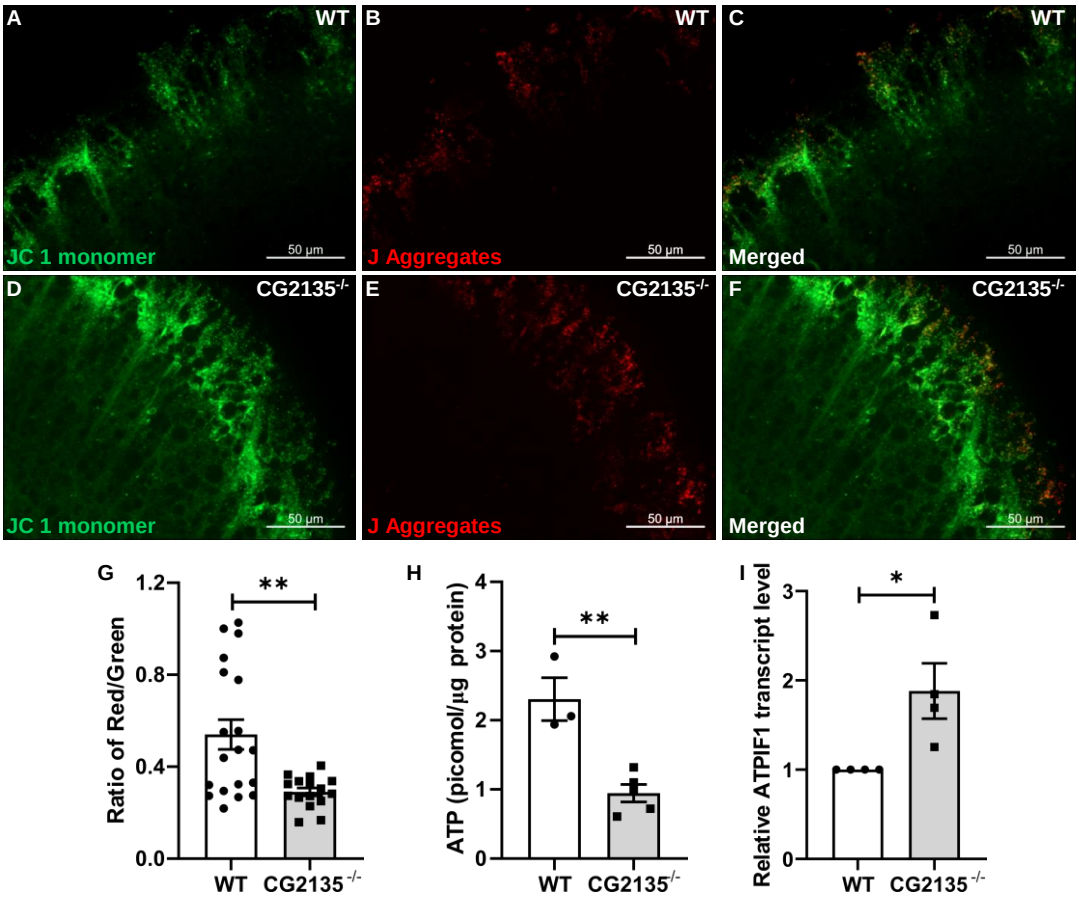
A
WT
JC 1 monomer
50 µm
B
WT
J Aggregates
50 µm
C
WT
Merged
50 µm
D
CG2135-/-
JC 1 monomer
50 µm
E
CG2135-/-
J Aggregates
50 µm
F
CG2135-/-
Merged
50 µm
G
Ratio of Red/Green
1.2
0.8
0.4
0.0
**
WT
CG2135 -/-
H
ATP (picomol/µg protein)
4
3
2
1
0
**
WT
CG2135-/-
I
Relative ATPIF1 transcript level
3
2
1
0
*
WT
CG2135 -/-

Figure 6

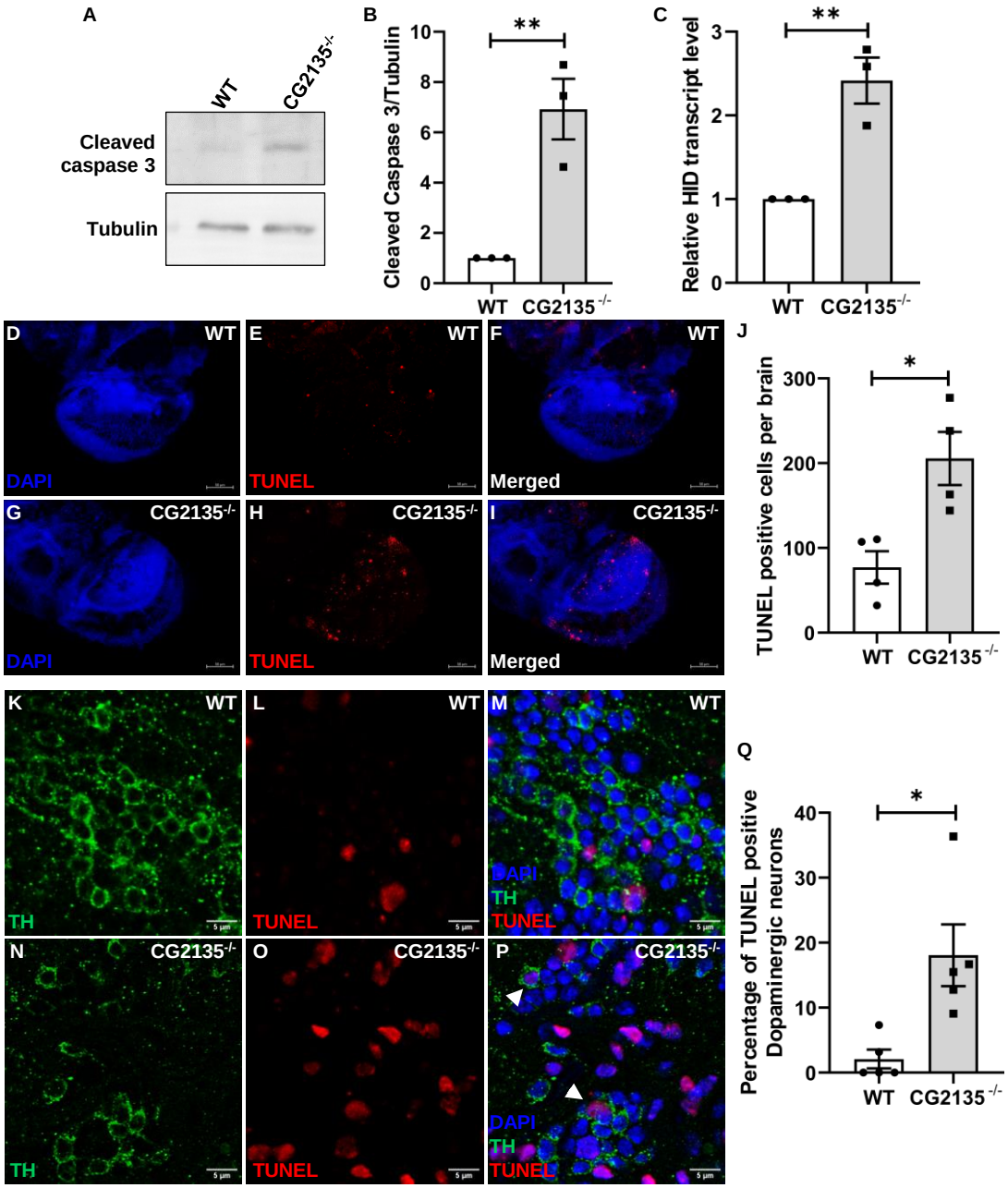
A
WT
CG2135-/-
Cleaved caspase 3
Tubulin
B
Cleaved Caspase 3/Tubulin
**
WT
CG2135-/-
C
Relative HID transcript level
**
WT
CG2135-/-
D
WT
DAPI
E
WT
TUNEL
F
WT
Merged
G
CG2135-/-
DAPI
H
CG2135-/-
TUNEL
I
CG2135-/-
Merged
J
TUNEL positive cells per brain
*
WT
CG2135-/-
K
WT
TH
L
WT
TUNEL
M
WT
DAPI
TH
TUNEL
N
CG2135-/-
TH
O
CG2135-/-
TUNEL
P
CG2135-/-
DAPI
TH
TUNEL
Q
Percentage of TUNEL positive Dopaminergic neurons
*
WT
CG2135-/-

Figure 7

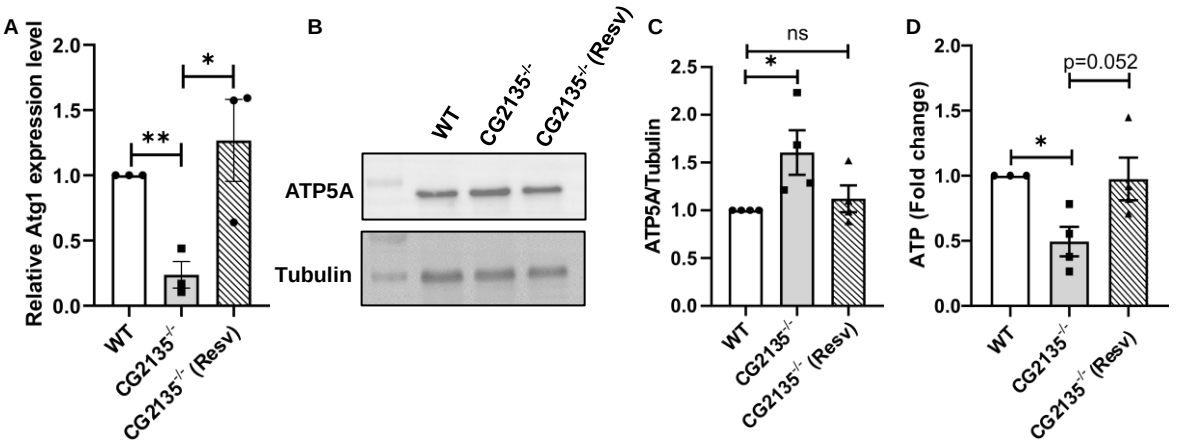
A
Relative Atg1 expression level
2.0
1.5
1.0
0.5
0.0
**
*
WT
CG2135-/-
CG2135-/- (Resv)
B
WT
CG2135-/-
CG2135-/- (Resv)
ATP5A
Tubulin
C
ATP5A/Tubulin
2.5
2.0
1.5
1.0
0.5
0.0
ns
*
WT
CG2135-/-
CG2135-/- (Resv)
D
ATP (Fold change)
2.0
1.5
1.0
0.5
0.0
p=0.052
*
WT
CG2135-/-
CG2135-/- (Resv)

Supplementary information

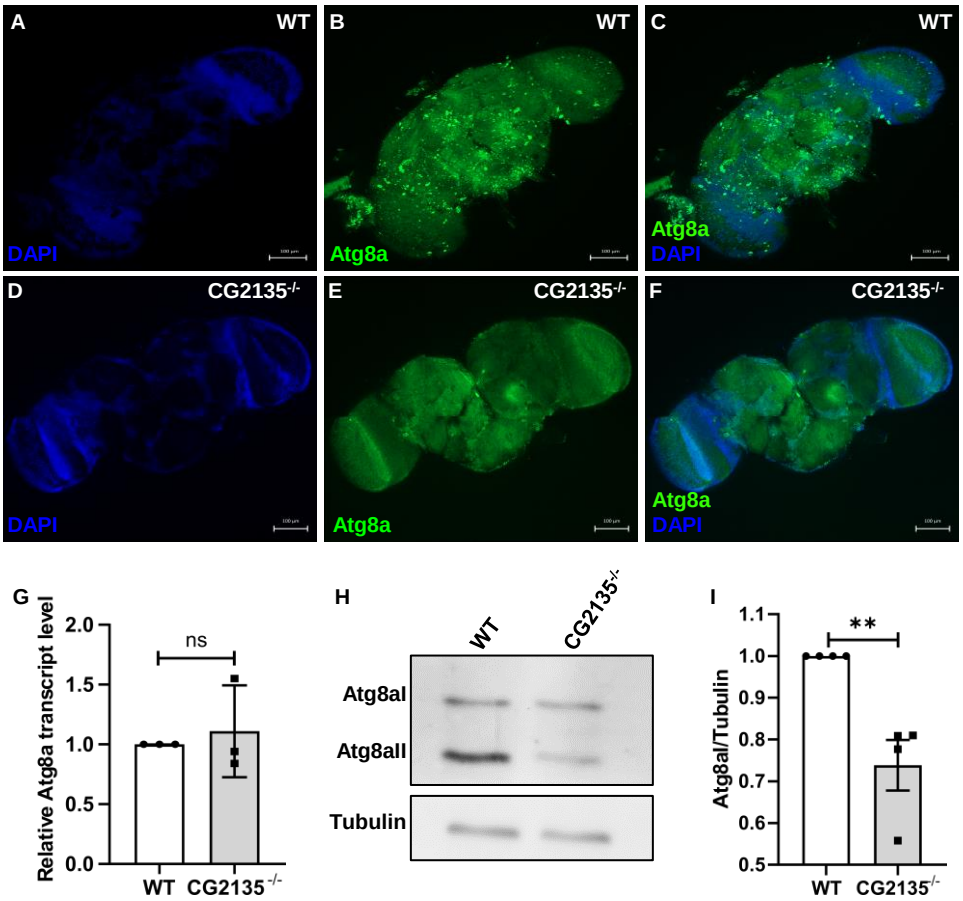

Figure S1: Reduced Atg8a in 30 days old CG2135$^{-/-}$ fly brain, Related to Figure 2

(A-F) The whole brain of 30 days WT and CG2135$^{-/-}$ was stained with anti-Atg8a (green) and counterstained with DAPI (blue), showing a low Atg8a signal in CG2135$^{-/-}$ brain compared to WT. Images taken in Apotome.2 (Carl Zeiss) and the tiles were reconstructed using Zen software. Scale bar represents 100µm.

(G) The bar graph represents the Atg8a transcript level in 30 days WT and CG2135$^{-/-}$ determined by RT-qPCR normalised to RP49 as housekeeping gene control. (N=3)

(H-I) Immunoblot of Atg8a for 30-day-old head lysate of WT and CG2135$^{-/-}$. Relative quantification of Atg8a-I/Tubulin intensity from immunoblot and tubulin kept as a loading control. (N=3)

All experiments were done independently. Error bars represent the standard error of the mean (SEM). Asterisks represent a level of significance (**$P \leq 0.01$, Student's *t*-test).

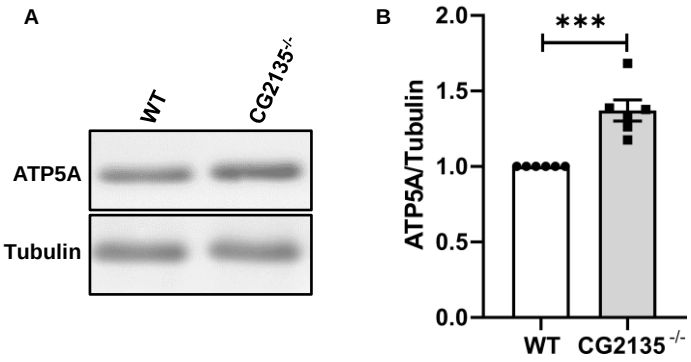

Figure S2: Western blot analysis of ATP5A protein, Related to Figure 3

(A-B) Western blot of mitochondrial protein ATP5A followed by quantification of the data shows an increased abundance of ATP5A in ≥30 days CG2135$^{-/-}$ fly brain sample, suggesting increased accumulation of mitochondria. (N=6)

All experiments were done independently. Error bars represent the standard error of mean (SEM). Asterisks represent a level of significance (***$P \leq 0.001$, Student's *t*-test).

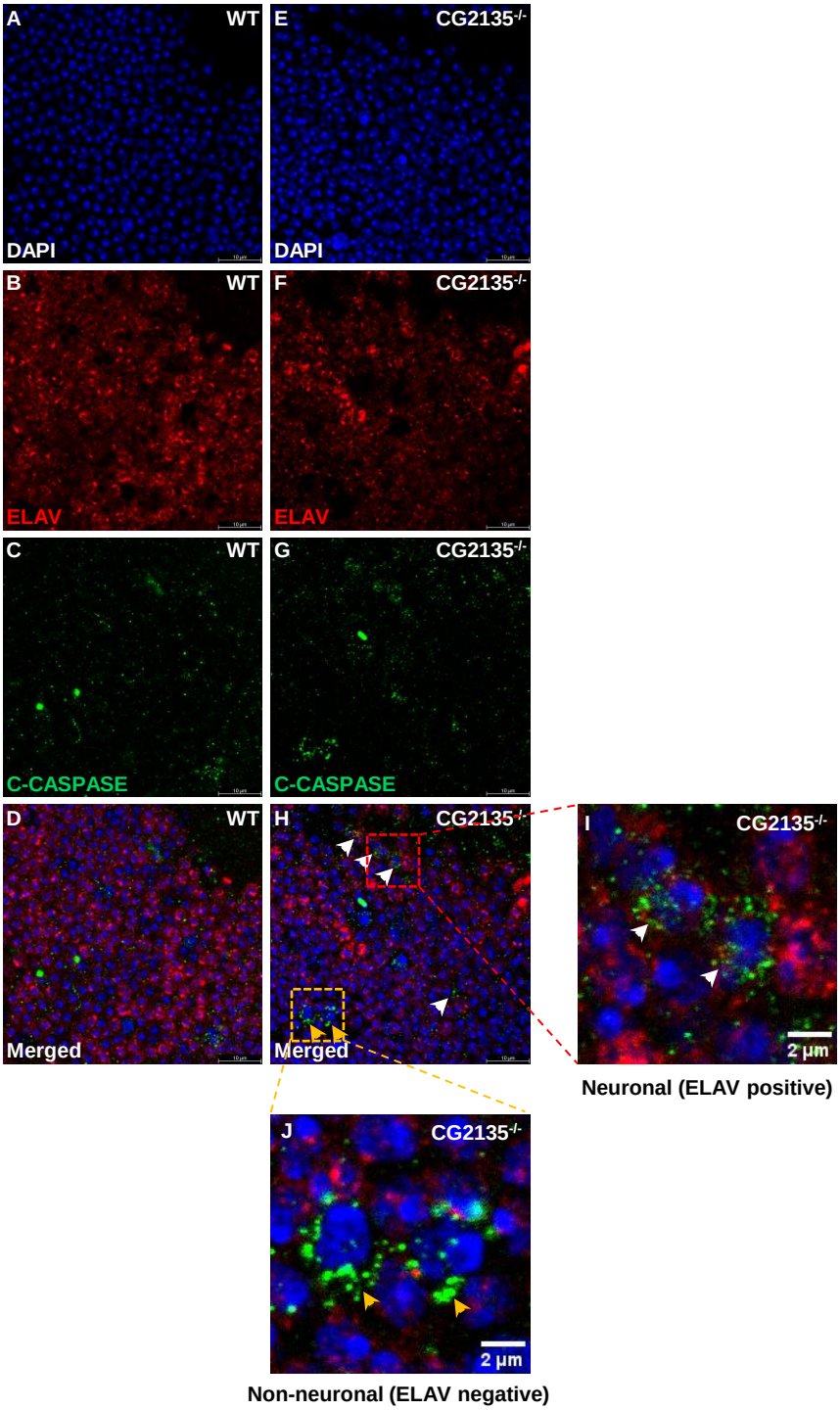

Figure S3: Accumulation of cleaved caspase3 positive cells in 45 days old CG2135$^{-/-}$ fly brain, Related to Figure 6

(A-H) Co-immunostaining with anti-Cleaved caspase 3 and anti-ELAV showed ELAV positive cells (pan-neuronal) are Cleaved caspase 3 positive cells (white arrow). A few non-ELAV cells are also Cleaved-caspase 3 positive (yellow arrow).

(I-J) Zoomed image showing ELAV positive (white arrow) pan-neuronal as well as non-Elav (yellow arrow) cells are cleaved caspase 3 positive suggesting a global apoptosis activation.